ANNUAL REVIEWS

Annual Review of Fluid Mechanics

Liquid-State Dewetting of Pulsed-Laser-Heated Nanoscale Metal Films and Other Geometries

Lou Kondic,[1] Alejandro G. González,[2] Javier A. Diez,[2] Jason D. Fowlkes,[3,4] and Philip Rack[3,4]

[1]Department of Mathematical Sciences and Center for Applied Mathematics and Statistics, New Jersey Institute of Technology, Newark, New Jersey 07102, USA; email: kondic@njit.edu

[2]Instituto de Física Arroyo Seco (CIFICEN-CONICET-CICPBA), Universidad Nacional del Centro de la Provincia de Buenos Aires, 7000 Tandil, Argentina

[3]Nanofabrication Research Laboratory, Center for Nanophase Materials Sciences, Oak Ridge National Laboratory, Oak Ridge, Tennessee 37831, USA

[4]Department of Materials Science and Engineering, University of Tennessee, Knoxville, Tennessee 37996, USA

Annu. Rev. Fluid Mech. 2020. 52:235–62

First published as a Review in Advance on August 19, 2019

The *Annual Review of Fluid Mechanics* is online at fluid.annualreviews.org

https://doi.org/10.1146/annurev-fluid-010719-060340

Keywords

thin metal films, fluid instabilities, laser heating, thermal effects, disjoining pressure

Abstract

Metal films of nanoscale thickness, deposited on substrates and exposed to laser heating, provide systems that involve several interesting multiphysics effects. In addition to fluid mechanical aspects associated with a free boundary setup, other relevant physical effects include phase change, thermal flow, and liquid–solid interactions. Such films are challenging to model, in particular because inertial effects may be relevant, and large contact angles require care when considering the long-wave formulation. Applications of nanoscale metal films are numerous, and the materials science community is actively pursuing more complex setups involving templated films and substrates, bimetallic films and alloys, and a variety of elemental film geometries. The goal of this review is to discuss our current understanding of thin metal film systems, while also providing an overview of the challenges in this research area, which stands at the intersection of fluid mechanics, materials science, and thermal physics.

1. INTRODUCTION

Metal films of nanoscale thickness are of interest in numerous applications involving metal particles and other geometries (films, filaments, and more complicated shapes), including solar cells, plasmonics-related applications, sensing, and detection, among others; readers are referred to Hughes et al. (2017) and Makarov et al. (2016) for recent application-centered reviews. In addition to their scientific interest, understanding these instabilities and the subsequent material transport is further motivated by their potential to drive various self- and directed-assembly mechanisms in a variety of contexts; only some examples are cited here (Ross 2010, Favazza et al. 2006b, Xia & Chou 2009, Krishna et al. 2010, Fowlkes et al. 2014, Reinhardt et al. 2013). Many technological applications, such as high-density data storage (Xia & Chou 2009), require the resulting ordered and robust assemblies of nanoparticles. The possibility of generating a complex ordered structure from this evolution has been of interest for technological applications such as solar cells and next-generation computer chips (Garnett et al. 2011, Mokkapati & Catchpole 2012).

Solid-state dewetting, whereby thin solid films and nanostructures are unstable at temperatures well below melting, has been studied for decades. The dewetting occurs via surface diffusion dictated by surface energy minimization and competing grain growth, as well as residual stresses in the film (Thompson 2012). Analogous to solid-state dewetting, pulsed-laser-induced dewetting (PLiD) has recently been explored as a synthesis technique in which thin metallic films or lithographically patterned nanostructures are irradiated with a nanosecond pulsed-laser source sufficient to melt the thin films. Conveniently, the nanoscale thickness roughly equals the absorption depth of ultraviolet/visible radiation, providing an opportunity to efficiently deposit energy in patterned metal films via pulsed-laser sources, which can provide predictable and homogeneous metal film heating. The relatively large laser beam area, with an edge dimension of 10^{-2} m, compared to a patterned film dimension on the order of 10^{-7} m, makes it possible to uniformly irradiate the film. This typically minimizes energy gradients in the in-plane coordinate. Pulsed lasers provide a way to rapidly elevate the metal film temperature. Liquid-phase temperatures (10^3 K) may be achieved owing to relatively small film volumes using high-power laser irradiation, and the resulting liquid lifetimes occur on timescales comparable to the pulse duration.

Post–laser irradiation imaging is typically performed to characterize the resultant nanoscale morphology of a PLiD experiment. Scanning electron microscopy (SEM) is most commonly used because the features are typically too small for optical microscopy. The dewetting evolution and final nanoparticle size and spacing can be captured in a plane view, while the wetting angle can be captured via tilt or cross-sectional imaging. Atomic force microscopy can be used to complement SEM analysis, making it possible to resolve curved nanoparticle surfaces with high resolution, albeit with slower image acquisition times.

Figure 1 schematically illustrates the typical PLiD setup where an excimer laser (KrF or ArF) or a solid-state [Nd–YAG (neodymium-doped yttrium aluminum garnet)] laser source of typical energy density, 10^3–10^4 J/m^2, is used to irradiate a thin metal film. **Figure 1** a is a cross-sectional view illustrating a laser pulse propagating toward a metal pattern/film, where the highlighted area is magnified for the case of a patterned filament (**Figure 1*b*,*c***) and a continuous film (**Figure 1*d*,*e***). The liquid lifetime is estimated as the time above the melting temperature and depends on the fluence and the thermophysical properties of the metal film and the substrate (see, e.g., McKeown et al. 2012). The rapid resolidification quenches in the fluid morphology, and thus multiple lower-fluence pulses can reveal temporal information about the fluid evolution. In this review, we focus on the experimental results obtained via nanoscale laser pulses; readers are referred to Makarov et al. (2016) for a discussion of experimental results obtained via femtosecond lasers and to Ye et al. (2018) for a more detailed discussion of both femtosecond and nanosecond laser pulsing with a focus on nanophotonics.

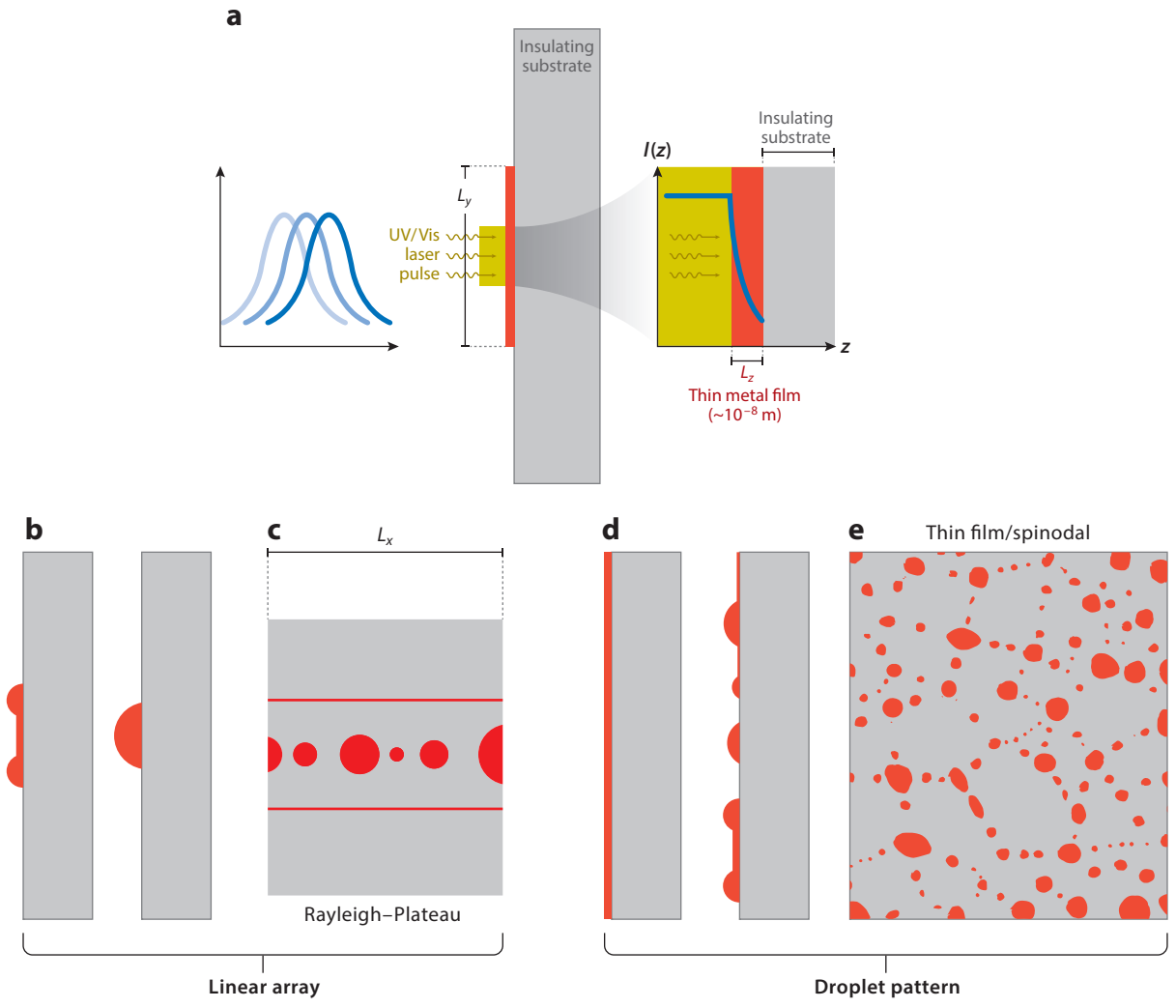

Figure 1

The pulsed-laser-induced dewetting scheme. (*a*) A thin metal film (*red*) of thickness $L_z \approx 10^{-8}$ m is irradiated with a 10^{-8} s ultraviolet/visible spectrum (UV/Vis) laser pulse. The radiant exposure of the film, $I(z)$, is approximately 10^3 mJ/m^2 and decays rapidly during propagation through the absorbing metal film. The absorption depth in the metal in the UV/Vis optical range is on the order of the metal film thickness. (*b–e*) The metal melting temperature is easily achieved for the case of a metal film supported on an insulating substrate (*gray*), and liquid-phase dewetting ensues. Metal film geometry can be specified using lithography. For example, (*b*,*c*) a linear array of solidified droplets forms as the result of the development of fluid instabilities when a metal film strip is defined during lithography; alternatively, for a deposited film, one finds a droplet pattern (*d*,*e*).

The outlined setup is clearly challenging, from not only experimental but also modeling and computational points of view. The considered systems evolve on a fast timescale and experience a rapid change of temperature and a resulting variation of material parameters; various instabilities that occur are influenced by the liquid film–solid substrate interaction, which has to be considered. Contact angles for liquid metals on SiO_2 substrates are large (e.g., 70–80° for Ni and Cu), making modeling and computations challenging in many cases of interest.

Table 1 Physical parameters of two typical fluids used in dewetting experiments

	ρ	μ	γ	τ	*Re*	*Ca*	*Oh*
Cu[a]	7.9	4.38×10^{-4}	1,781	2×10^{-8}	9.02×10^{3}	1.23×10^{-3}	3.69×10^{-4}
PS[b]	1.05	1.2×10^{3}	30.8	10^{3}	8.75×10^{-15}	3.90×10^{-6}	2.11×10^{4}

The variables ρ, μ, γ, and τ are in CGS (centimeter-gram-second) units, while *Re*, *Ca*, and *Oh* are dimensionless. The chosen length scale is $\ell = 1\,\mu$m. Abbreviations: *Ca*, capillary number; Cu, copper; *Oh*, Ohnesorge number; PS, polystyrene; *Re*, Reynolds number; γ, surface tension; μ, viscosity; ρ, density; τ, characteristic time.

[a]From González et al. (2013).

[b]From Becker et al. (2003).

Clearly, a multiscale, multiphysics approach is needed to make progress in understanding the considered setup. We start by discussing the basic features of the problem from a fluid mechanical viewpoint, starting by introducing some of the basic parameters and related nondimensional numbers. **Table 1** shows the most relevant physical parameters of a typical liquid metal such as copper. Since all fluid dynamics phenomena of interest to this problem occur on a timescale comparable to the pulse duration, t_p, the characteristic timescale of the problem, τ, can be estimated as t_p. This very short timescale is a distinguishing feature of liquid metals at the nanoscale, thus making any real-time observation of their evolution difficult.

To introduce the relevant scales and dimensionless parameters, we specify a typical out-of-plane scale, h_0, describing the metal thickness, as well as an in-plane length, ℓ, which may be defined by either the wavelength of the film instability (similar but not necessarily the same as the distance between drops/holes) or geometrical features of a patterned film. Based on these two length scales, one can define $\epsilon = h_0/\ell \ll 1$. Focusing first on the in-plane length scale, one can define the in-plane Reynolds number, $Re = \rho\ell^2/(\tau\mu)$; capillary number, $Ca = \mu\ell/(\tau\gamma)$; and Ohnesorge number, $Oh = \mu/\sqrt{\rho\gamma\ell}$. **Table 1** specifies the numerical values. Note that *Re* is large, while *Ca* and *Oh* are very small. This may suggest that inertial effects may have important effects for metals. However, one could argue that the out-of-plane length scale should be considered instead; in this case, for a typical value $\epsilon = 10^{-2}$, one finds that the reduced Reynolds number is given by $Re' = \epsilon^2 Re \approx 1$, indicating that inertial effects may have marginal effects only (González et al. 2016). Below we discuss the setups where inertial effects are either almost irrelevant or dominant, as the relevance of inertial effects may also depend on a particular problem in question.

It is worth comparing the nondimensional numbers with those relevant for polymeric thin films, since such films have been studied thoroughly. **Table 1** includes the corresponding physical parameters for polysterene (PS). While *Ca* also remains small for PS, *Re* and *Oh* change in the opposite direction compared to the Cu values due to the high value of the polymer viscosity. Therefore, even if there are some similarities between metal and polymer films, there are also significant differences that should be taken into account when modeling their respective fluid dynamics.

Finally, let us introduce a concept discussed in more detail in Section 3: the timescale, τ_s, corresponding to the growth of the fluid mechanical instabilities of a thin film due to the liquid–solid interactions described in the next section. For films of thickness 5 nm, the relevant timescales are $\approx 10^3$ s for a PS film and 10^{-9} s for a Cu (or similar metal) film. While these timescales differ by 12 orders of magnitude, they are both comparable to the typical experimental timescales, suggesting that in both cases, fluid mechanical types of modeling are appropriate.

This review is structured as follows. Since we have already provided the basic description of the experimental setup, in Section 2 we discuss modeling and computational approaches. As liquid–solid interaction forces are crucial for understanding the problems in question, we start by describing their inclusion into fluid mechanical models. We then proceed by discussing modeling

approaches within the long-wave (LW) formulation (for small slopes), which, as we will see, is useful despite the large contact angles typically involved, in addition to phase change and thermal effects. Section 2.4 focuses on computational methods implemented within the LW formulation, approaches used for direct numerical simulations of the Navier–Stokes (NS) equations, and molecular dynamics (MD) approaches. Sections 3 and 4 focus on the two most commonly considered geometries, thin films and filaments, respectively. We conclude by discussing some of the open problems in Section 5.

2. MODELING AND COMPUTATION

2.1. Liquid–Solid Interaction

The nanoscale dimensions of interest suggest that the interaction between the liquid metal and the solid substrate is relevant. The liquid metal–solid substrate interaction forces are often described by the so-called disjoining pressure, Π, whose dependence on the film thickness, h, involves competition between long- and short-range forces [see Bonn et al. (2009) for a recent review]. The disjoining pressure plays a crucial role in determining the stability of thin films. This pressure term encompasses a variety of effects that take into account both repulsive and attractive forces between molecules or atoms and between electrons in a metallic liquid.

When considering liquid metal–solid substrate interaction, the simplest approximation is to consider London forces between atoms or molecules that are separated by a distance r. This force takes into account the instantaneous quantum dipole fluctuations of a neutral atom and has a r^{-6} law for pair interactions between this dipole and the induced one in other atoms (Israelachvili 1992, Parsegian 2006). However, a more detailed study requires refining the expressions used to describe the disjoining pressure. Usually van der Waals forces are considered and some mean macroscopic law is obtained. From these elements, it is possible to obtain an expression of the disjoining pressure (Israelachvili 1992, Parsegian 2006, Butt & Kappl 2010).

Exponential and inverse power laws have been used in polymeric liquids, where there is a clearer picture and experiments are easier to control than with liquid metals. It is generally assumed that the corresponding laws for liquid metals are similar, but perhaps with different exponents in the power laws. In general, the comparisons between different theoretical laws and experiments have not been quite systematic. Most of them have relied on a particular power law and are of an indirect nature: either attempting to observe equilibrium states (Derjaguin et al. 1985) or some instability patterns related to the disjoining pressure effects (González et al. 2013).

The exact functional form of Π is not known for liquid metals since many effects can be present in the problem (thus leading to different laws) and direct measurements are not available (Ajaev & Willis 2003, Wu et al. 2010, Ajaev 2013). However, the expression that is most commonly used is (Mitlin 1994, Schwartz 1998, Mitlin 2000)

$$\Pi(h) = \kappa f(h) = \kappa \left[\left(\frac{h_*}{h} \right)^n - \left(\frac{h_*}{h} \right)^m \right], \qquad 1.$$

where $n > m$ are positive exponents and h_* is the equilibrium thickness at which repulsive and attractive forces balance. The pressure scale, κ, is related to the Hamaker constant, A, as $A = 6\pi\kappa h_*^3$. In the literature, only a small subset of exponents (n, m) have been considered. Typical examples (Craster & Matar 2009) for polymeric films are (9, 3), (4, 3), and (3, 2). For liquid metals, some of these exponents have also been used or simplified versions with attractive forces only have been used (Favazza et al. 2006a, Trice et al. 2008, Krishna et al. 2009). More complex models with an additional exponential term (Krishna et al. 2010) have been considered as well.

One approach is to consider Lennard–Jones potentials for the interaction between atoms,

$$U(r) = 4U_0\left[\left(\frac{\sigma}{r}\right)^{12} - \left(\frac{\sigma}{r}\right)^{6}\right], \qquad 2.$$

where U_0 is the depth of the potential, σ is the atomic radius, and r is the distance between the atoms. To obtain the disjoining pressure term, one integrates the interactions over an infinitely extended substrate and on a liquid column of height h and unit cross-sectional area (Israelachvili 1992, Butt & Kappl 2010). According to the model used in Equation 2, the resultant interaction energy of a single particle in the liquid with all the particles in the substrate can be written as $\mathcal{V} = \int_{\Omega_S} U n_s \, d\Omega$, where Ω_S is the substrate volume and n_s is the number of particles per unit volume in the substrate. Taking a derivative of this energy (per unit area), one obtains the disjoining pressure of the functional form specified by Equation 1 with $n = 9$ and $m = 3$, and with $h_* = (2/15)^{1/6}\sigma$ being the thickness at which $\Pi(h_*)$ goes to zero. Additionally, κ is given by $\sqrt{10/3}\pi n_l n_s U_0 \sigma^3$, where n_l is the number of particles per unit volume of liquid. This model may be useful for comparing with MD simulations where one wants to keep the interaction laws to a minimal simple form using pairwise Lennard–Jones interactions between identical molecules and to emphasize the large number of interactions (Nguyen et al. 2012).

Although simple, this approach is not always useful, since realistic situations require several additional considerations. First, the van der Waals forces are not additive in general. This is particularly true for liquids formed by polarized molecules. Moreover, due to retardation effects, the usual inverse power laws for the van der Waals forces may change as distance from a molecule is increased. Further effects may be due to Casimir forces in metallic films (Butt & Kappl 2010) illuminated by lasers. The studies based on Lifshitz theory (Israelachvili 1992) have demonstrated that van der Waals or Casimir forces can be modified due to a change of the optical properties of the materials (Arnold et al. 1979, Vogel et al. 1992, Chen et al. 2007, Inui 2007, Chan et al. 2008, Klimchitskaya et al. 2009, Bao et al. 2010). This change can be produced by the generation of extra free electrons due to the laser irradiation that may take place in metal liquid experiments.

Besides the laser effect, an increased temperature that may smear the electronic distribution around the Fermi energy can also modify the liquid metal optical constant. Due to all of these effects, general laws describing the interaction of melted metals with substrates are extremely difficult to obtain from first principles. Nevertheless, several attempts have been made to deduce the appropriate laws by using drastic simplifications that may or may not apply to a particular experimental setup. Notably, Derjaguin et al. (1985) have attempted to obtain expressions for the electronic contribution, Π_e, to the disjoining pressure by taking into account the interactions of electrons with one another and with ions. In order to do that, they use several simplifying assumptions to obtain $\Pi_e \propto h^{-2}$. This result assumes an averaging over several atomic lengths and assumes that the film is thin enough to ensure that $(1/h)(hS/N)^{1/3}$ is small, where S is the surface area and N is the total number of electrons in the film. The resulting disjoining pressure was compared with that produced by the molecular attraction forces that are assumed to vary as $\Pi_m \propto h^{-5}$ (Landau & Lifshitz 1980). They concluded that both attractive and repulsive effects are relevant.

Since it is unclear from the literature which exponents apply for each particular case, one possibility is to use the simple model specified by Equation 1 with various sets of exponents and to verify that they provide consistent results. Then, one could identify the pair that provides the best agreement with the experimental results, while remembering that the functional form specified by Equation 1 is an approximation itself. We discuss applications of this approach in Section 3.

2.2. Fluid Mechanical Models

The most obvious approach to modeling the evolution of metal films and other geometries is based on the NS equations. However, this approach is not the simplest one since one needs to deal with a complicated free boundary problem leading to computational difficulties, in addition to including liquid–solid interaction forces and dealing with possible topological changes of the fluid geometry. Due to all of these complexities (which we discuss further in Section 2.4), a significant amount of modeling work has been carried out within the LW formulation, despite the fact that contact angles of interest are typically large and therefore LW is not always easy to justify.

Within the asymptotic LW formulation, one uses the fact that the relevant metal geometries are thin; one can simplify the problem considerably by carrying out a systematic expansion in terms of the small parameter, ϵ, which describes the ratio of relevant out-of-plane and in-plane length scales. LW has been used widely for several problems, and excellent reviews are available (see Oron et al. 1997 and Craster & Matar 2009). It is also worth mentioning that there is a variety of approximations that account for, for example, the relevance of inertial effects [discussed extensively by Craster & Matar (2009) and González et al. (2016)] or include modifications due to large contact angles (Snoeijer 2006). Here we stick to the basic formulation; after carrying out the LW expansion, including liquid–solid interaction forces via disjoining pressure but excluding gravity effects due to the short length scales in question, we are led to the following fourth-order nonlinear partial differential equation (PDE) for the film height (see, e.g., Burelbach et al. 1988),

$$\frac{\partial h}{\partial t} + \nabla \cdot (h^3 \nabla \nabla^2 h) + K \nabla \cdot [h^3 f'(h) \nabla h] + D \nabla \cdot (h^2 \nabla T) = 0. \qquad 3.$$

Here, ∇ stands for $(\partial/\partial_x, \partial/\partial y)$, and (x, y) are the in-plane coordinates. The second term is due to surface tension (with pressure proportional to the film curvature, which is approximated by $\nabla^2 h$), and the remaining two terms are due to the liquid–solid interaction (already discussed in Section 2.1) and the Marangoni effect, respectively. The latter results from the temperature dependence of the liquid–air surface tension, which is typically assumed to be of the form $\gamma(T) = \gamma_0 + \gamma_T T$, where γ_0 equals $\gamma(T_0)$ and γ_T is (for most of the materials including metals) a negative constant, with T_0 being some reference temperature. Next, we define $t_s = 3\mu l_s/\gamma_0$ as the timescale, where l_s is a chosen length scale (typically one uses film thickness for this purpose, i.e., $l_s = h_0$). The nondimensional parameters are then specified by $K = \kappa l_s/\gamma_0$ and $D = 3\gamma_T/(2\gamma_0)$. The reader is referred to Diez & Kondic (2007) for an extensive discussion of including disjoining pressure in the LW framework; to Trice et al. (2007), Kondic et al. (2009), and González et al. (2013) for the use of the LW framework in modeling liquid metal films; and to Oron et al. (1997), Colinet et al. (2001), and Craster & Matar (2009) for discussions of Marangoni effects in a variety of settings.

2.3. Phase Change and Thermal Effects

The process of heating and melting metal films has been modeled by considering heat transport via diffusion mechanisms through the metal film and underlying substrate. One particular aspect of modeling heat flow for nanoscale metals is that the adsorption depth for the laser source is often comparable to the film thickness, and therefore the amount of absorbed energy depends on the local metal thickness. In addition, reflectivity of the metal film depends on its thickness as well (Trice et al. 2007). The film thickness itself may be influenced by the temperature through variations in the material's parameters (such as viscosity, density, and surface tension). All of these complexities have motivated the development of various simplified methods. Trice et al. (2007)

considered a one-dimensional model for heat propagation (heat transfer only in the out-of-plane direction), while also decoupling heat transfer from the film evolution. This and other works (Atena & Khenner 2009, Fowlkes et al. 2011) have shown that the timescale on which a metal film remains in the liquid state is comparable to the duration of the pulse. However, the picture of modeling heat flow is still not complete; for example, Trice et al. (2007) noted that including thermal resistance of the metal–solid interface using known values for thermal resistance leads to erroneous results. Furthermore, the effects of radiative heat losses are not well understood, to mention just a few modeling issues related to heat flow. Clearly, much more work needs to be done in this direction.

Going back to the existing models, Marangoni effects have been analyzed within the framework of the LW approach, leading to additional terms in the evolution equation, as discussed in Section 2.2. While some works (Trice et al. 2008, Dong & Kondic 2016) have suggested that Marangoni effects may have a significant influence, more careful modeling within the NS framework coupled with heat diffusion, which also includes heat transfer in the in–plane direction (Seric et al. 2018a), has suggested that simplified modeling may be overestimating the Marangoni effect since it leads to artificially high temperature gradients. The influence of the temporal change of material parameters (such as surface tension) was found to be much more significant. In other words, it was found that the balance of normal stresses at the metal–air interface is much more relevant than the balance of tangential ones; for more detailed discussion regarding normal and tangential stresses and their influence on the dynamics, readers are referred to reviews by Oron et al. (1997) and Craster & Matar (2009). The amount of research in this direction is so far limited in the context of liquid metal films on nanoscale, and more effort is needed to understand and perhaps exploit the influence of thermal effects.

Another related aspect involves the phase change between solid and liquid. Modeling efforts in this direction and in the context of nanoscale metals is very sparse (Trice et al. 2007, Fowlkes et al. 2011). One aspect of the problem that is relevant from the modeling point of view is that the substrate itself can be transparent to laser irradiation, so that the heating of the system essentially progresses by heating the metal via absorption, to be followed by heat transfer via diffusion through the substrate. Typically, it is assumed that the substrate itself remains solid; however, there are experimental indications (Kondic et al. 2009) that this may not always be the case. More careful modeling of melting and solidification (Font et al. 2017, Ahmmed & Huda 2018) has suggested that the substrate itself may partially melt, becoming either a soft solid or viscous liquid. Such a setup, in which the substrate itself evolves, requires more careful modeling of fluid dynamics on soft, evolving solids, which is a research topic of relevance in several other applications of micro- and nanofluidics, as discussed by Andreotti & Snoeijer (2020) in this volume.

2.4. Computing Techniques

The computing methods used for simulating thin metal films can be separated into three broad categories: methods based on LW models, direct simulations that solve NS equations, and MD simulations. In what follows, we discuss briefly each of these categories.

2.4.1. Computing within the long-wave model. The LW approach leads to a fourth-order nonlinear PDE for the film thickness that needs to be solved. Various numerical methods have been developed based on finite-difference, finite-element, spectral, or other discretization techniques. The literature discussing various computational advances is extensive, and we do not attempt to review it here. However, it is worth mentioning new advances (with the source codes publicly available) that allow for simulations of large computational domains (Wilczek et al. 2017,

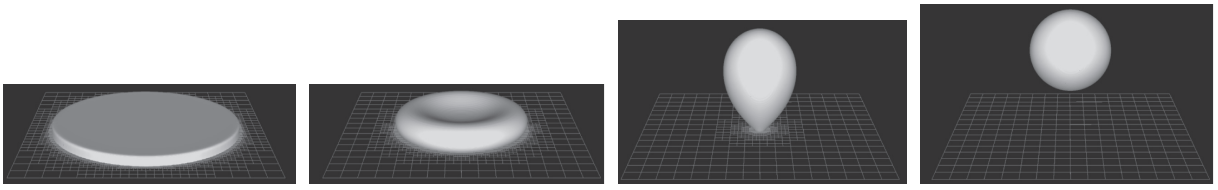

Figure 2

Evolution of a liquid metal disk with an initially imposed contact angle of $\theta_0 = 90^\circ$ and an equilibrium contact angle of $\theta_{eq} = 140^\circ$. (*Lower left*) The disk detaches from the substrate due to strong inertial effects. Figure adapted from Afkhami & Kondic (2013).

Lam et al. 2018a), which make it possible to carry out statistically significant data analysis and discuss the evolution of various features of the solutions (instabilities and similar features) with minimized boundary effects.

As with the direct numerical solvers discussed below, metal film instabilities are crucially dependent on the liquid–solid interaction forces and therefore need to be explicitly taken into account to ensure that the relevant instability mechanisms are captured. Additionally, disjoining pressure allows one to define the contact angle in a natural way (see, e.g., Diez & Kondic 2007). Note that if a contact line is already present in the problem due to the initial geometry (such as for filaments or rings), an alternative approach to disjoining pressure inclusion is to relax the no-slip boundary condition with the specified contact angle.

2.4.2. Direct numerical solutions. Many methods have been used to solve the NS equations with a moving interface, including level set and volume of fluid methods (Sussman et al. 1999, Renardy & Renardy 2002, Spelt 2005, Francois et al. 2006, Afkhami et al. 2009, Popinet 2009, Sussman & Ohta 2009), phase field methods (Jacqmin 2000, 2004; Sibley et al. 2013), and lattice Boltzmann methods (Briant et al. 2004, Lee & Liu 2010). Since such problems are common in a variety of fluid mechanical problems, there are open source computational packages, such as Gerris or OpenFOAM. **Figure 2** shows an example of simulations (Afkhami & Kondic 2013) using the Gerris package based on the volume of fluid approach to simulate the dramatic evolution of gold particles on substrates, considered in experiments by Habenicht et al. (2005). Here, one observes that strong inertial effects in the considered geometry lead to detachment of the particles from the substrate. While we focus in this review on the configurations where the evolution is significantly slower and the topological changes presented in **Figure 2** do not occur, it is encouraging that this type of dynamics can be captured and that MD simulations (Fuentes-Cabrera et al. 2011a) find similar results.

While simulations used to produce the detachment shown in **Figure 2** are successful in capturing the fast evolution of this strongly out-of-equilibrium configuration, they are incomplete in the sense that they do not explicitly include the liquid–solid interaction. This inclusion is crucial if one wants to consider thin film instabilities and the resulting dewetting. Two approaches have been considered, both within the framework of the volume of fluid method: inclusion via volume forcing (Mahady et al. 2015a) and via surface forcing (Mahady et al. 2016). It turns out that the latter approach is significantly more efficient and that it produces converged results for three-dimensional films that are significantly larger in the in-plane directions than a typical distance between the drops; some results of the simulations based on this model are discussed in Section 3.3. Another important issue is the inclusion of Marangoni effects; this task has been addressed recently as well (Seric et al. 2018a).

2.4.3. Molecular dynamics computations. The small spatial scales of the considered systems and the importance of liquid–solid interaction forces suggest that MD-type simulations could provide useful insights. However, despite the small scales, simulations of the system extended in more than one spatial dimension are computationally extensive and require supercomputers, as implemented in the context of liquid crystals (Nguyen et al. 2014). The MD problem of a free nanoscale cylinder has recently been compared with several fluid models (Zhao et al. 2019). Within the context of liquid metals, existing MD simulations (Fuentes-Cabrera et al. 2011b; Fowlkes et al. 2012a; Nguyen et al. 2012, 2014) have included the interaction between metal and substrate atoms with a truncated Lennard–Jones potential and have led to results consistent with the continuum simulations. Due to the significant computational resources required, at this point, MD simulations and nanoscale experiments are still carried out on different length and timescales. To some degree, it is the task of continuum simulations, which can be carried out on both scales, to bridge between MD and experimental scales of relevance.

3. THIN FILMS AND RELATED GEOMETRIES

The stability of thin nanoscale films has been considered extensively in the context of polymer films [see Craster & Matar (2009) for a review of this topic]. Although the slow evolution of instabilities for nanoscale polymer films provides insights, there has been an intense discussion of various instability mechanisms, such as spinodal dewetting and homogeneous and heterogeneous nucleation (Herminghaus et al. 1998, Seemann et al. 2001, Becker et al. 2003, Sharma & Verma 2004, Fetzer et al. 2005, Münch & Wagner 2005, Jacobs et al. 2008). While satisfactory answers have been mostly reached in the case of polymer films, recent works (Lam et al. 2018a,b) have suggested that the influence of various instability mechanisms may be strongly influenced by the form of disjoining pressure. As discussed in Section 2.1, since the form of disjoining pressure is not known precisely (at least for the case of metal films), the instability mechanism itself is not always obvious. Of course, the fast evolution of metal films does not help, since it is challenging to observe film evolution experimentally. Despite these outlined limitations, in this section, we see that important insights can be reached using linear stability analysis (LSA) to carefully analyze the initial stages of instability in experiments and simulations to discuss nonlinear aspects of instability development.

3.1. Experiments

Discussions of the development of instabilities for thin metal films have been around since pioneering studies from the late 1990s (Bischof et al. 1996, Herminghaus et al. 1998). For laser-irradiated ultrasmooth Au, Cu, and Ni thin films on mica, Bischof et al. (1996) noted random holes attributed to nucleation and a high density of small holes with a correlated length scale attributed to spinodal instability. **Figure 3** shows more recent experimental results from Krishna et al. (2010). Visual analysis suggests that a spinodal mechanism may be important for thin films (**Figure 3*a–c***), while nucleation may play a role for thicker ones (**Figure 3*e–g***). Other works have suggested that the strength of laser exposure plays a role (either by changing the temperature or the liquid lifetime). Gurevich (2011) has shown that Voronoi-like cells whose size increases with laser pulse fluence appear for different metals. As one goes far from the center of the laser impact region, the size decreases for the same nominal fluence. Batič et al. (2017) studied Au films placed over either a flat Si surface or a previously structured substrate. Apparent spinodal patterns appear after annealing, evolving from holes with rims to drops. For structured substrates, aligned Au islands are formed with nonuniform sizes and elongated shapes confined by ridges. The authors claimed this result is similar to experiments performed on dewetting of thin metal lines, which

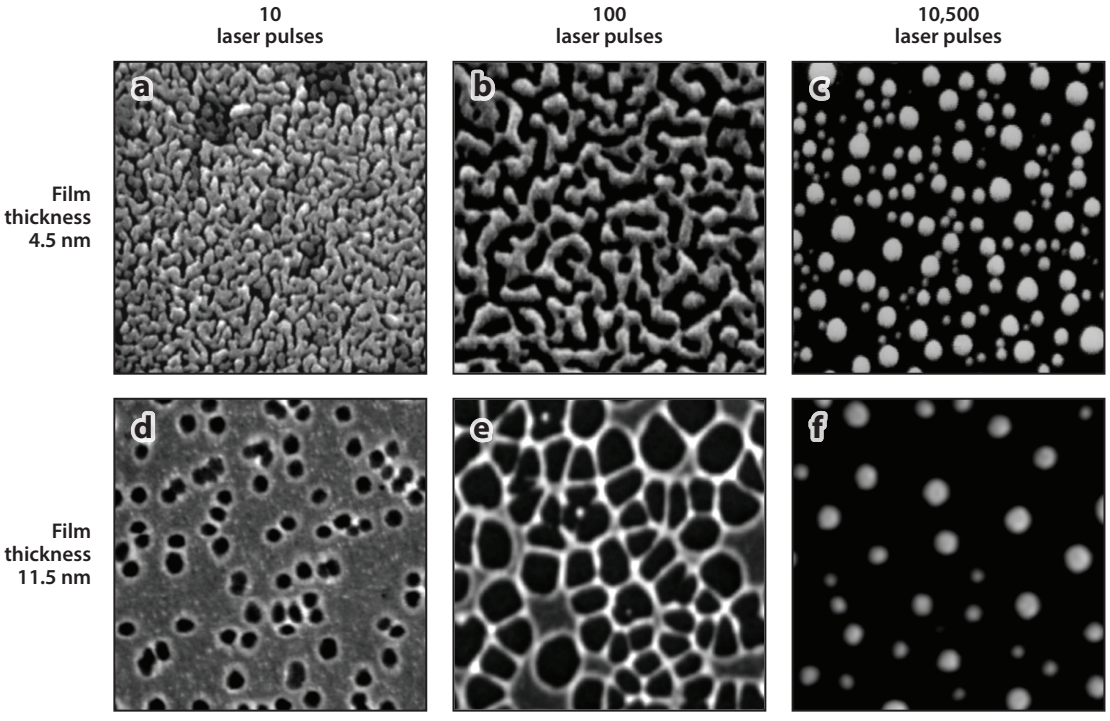

Figure 3

The initial Ag film thickness strongly influences the final morphology obtained in response to pulsed-laser-induced dewetting (Krishna et al. 2010). In these experiments, the semi-infinite Ag films were supported on SiO_2 substrates. (*a–c*) The time evolution of film morphology is estimated by conducting multiple experiments with an increasing number of laser pulses. In this example, (*a*) 10, (*b*) 100, and (*c*) 10,500 laser pulses were applied during three independent experiments. The final images acquired at each stage were then combined and considered as representative of the time evolution for a single experiment. (*d–f*) Hole evolution observed for films thicker than 11.5 nm. Images show the evolution at a film thickness of $h = 11.5$ nm. Figure adapted with permission from Krishna et al. (2010).

break down into small particles upon annealing by fluid instability. McKeown et al. (2012) also reported results consistent with spinodal dewetting and described the temporal evolution of Ni using a dynamic transmission electron microscope that employs a laser that is split into two beams and synchronized in the nanosecond time frame. One beam is directed at the photocathode to generate a beamlet of electrons that arrives synchronously with the second beam, which is directed at the substrate to heat the material. To our knowledge, this is the only work that reports the evolution of metal films of nanoscale thickness on the timescale measured in nanoseconds.

Favazza et al. (2006a,b) have performed several detailed studies of the self-assembly of nanoparticle arrays via PLiD, focusing on Co on SiO_2. They documented the evolution as a function of laser fluence and pulse number and correlated the particle size and spacing as functions of the film thickness. They also noted that the metal temperature may depend nonmonotonically on the film thickness: Thinner films do not absorb a sufficient amount of energy to reach high temperatures, while thick films require more energy than available to reach such high temperatures. Therefore, there is an optimum thickness at which the metal temperature reaches a maximum (see also Trice et al. 2007). Subsequent to these studies, the group investigated thicker films and found a sharp decrease in the spacing between resulting drops; this decrease was attributed to a (destablizing) Marangoni effect for thick films. However, as discussed in Section 2.3, it is not clear whether Marangoni forces actually play a role in instability development, so these experimental results may still be not well understood.

While the nanoparticle size and spacing have often been characterized as delineating whether spinodal dewetting or nucleation is operative (Ratautas et al. 2012, Ruffino et al. 2012b), some studies have also noted that the evolving holes combine to form rivulets that subsequently break apart by a Rayleigh–Plateau (RP)-type instability (Ruffino et al. 2012a). For instance, 10-nm-thick Cr films were studied and evolving ring-like structures were observed in SEM and atomic force microscopy images, where each ring was associated with a melt, liquid-phase retraction, and resolidification step per laser pulse (Lorenz et al. 2013). These signatures were useful in correlating the hole evolution as a function of laser intensity and pulse number.

While thin film and filament instabilities in air or in a vacuum have been extensively studied, there are compelling reasons to think that other media could lead to a more versatile nanoparticle assembly control. Bestehorn & Merkt (2006) suggested that a Rayleigh–Taylor-unstable thin film suspended on a substrate in equilibrium with its vapor phase under a steady-state thermal gradient can lead to patterns influenced by the evaporative process. Based on this idea, Yadavali & Kalyanaraman (2014) studied a system of an Au film and a substrate submerged in glycerol. The complex system consisted of various layers: a quartz substrate, a metal film, glycerol, and a gas (associated with the evaporated glycerol at the glycerol–gold interface). The resulting nanoparticle size and spacing was independent of film thickness within a range of 4 to 12 nm, in contrast to the h dependence for metal films on substrates without additional glycerol. The instability was described by the thickness-dependent pressure gradient that resulted from the evaporating glycerol at the heated gold–glycerol interface; thus, fluctuations in the melted gold film grew as material flowed from thin to thick regions. They argued that in their experiments this effect was more important than those due to disjoining pressure. Subsequently, Ruffino et al. (2016) compared the PLiD of thin gold films in glycerol versus air and found that the presumed Rayleigh–Taylor instability of the samples processed in glycerol had larger and more monomodal distributions, which were preferred for some plasmonic applications.

In addition to single-layer films, bilayer Ag–Co films have also been extensively studied (Krishna et al. 2011). This system is convenient because both solid and liquid phases of the components have limited solubility and so it can be treated theoretically as a simple two-layer immiscible system. Depending on the layer ordering, very different dewetting evolution pathways and length scales are observed since they are correlated with the signs of the intermolecular forces. The resultant bimetallic nanoparticles have been studied for their plasmonic (Garcia et al. 2012, Sachan et al. 2012) and so-called ferroplasmonic (Sachan et al. 2014) applications.

3.2. Linear Stability Analysis

In light of the discussion in Section 2.1, one possible use of LSA may be to reverse-engineer the experimental results and attempt to extract the parameters specifying disjoining pressure. Focusing on spinodal dewetting as the mechanism leading to instability, LSA of a thin film with disjoining pressure as specified by Equation 1 yields the following expression for the most unstable wavelength,

$$\lambda_{\mathrm{m}} = 4\pi h_*^2 \sqrt{\frac{3\gamma}{m\mathcal{A}} \left(\frac{h_0}{h_*}\right)^{m+1} \left[1 - \frac{n}{m}\left(\frac{h_*}{h_0}\right)^{n-m}\right]^{-1}}, \qquad 4.$$

where h_0 is the initial film thickness. Fast Fourier transforms and other image processing techniques can be helpful for understanding the operative instabilities. For example, one can correlate the initial hole mean distance and the final particle spacing with the liquid surface mode wavelengths responsible for their formation. The main finding reported by González et al. (2013) was

that, by taking into account the facts that (*a*) the value of the Hamaker constant should be in line with the results reported in the literature and (*b*) the equilibrium film thickness, h_*, should be in the reasonable range of a few angstroms, one could obtain good agreement between LSA and experiments only for $(n, m) = (3, 2)$ and not for the other commonly used pairs such as (4 ,3) and (9, 3) (the latter resulting from the Lennard–Jones potential). One interesting consequence of this is that using (3, 2) predicts that the most unstable wavelength, and therefore the distance between the hills and valleys that form during the film evolution, should scale as $h^{3/2}$, and not as h^2, as is usually expected and is found for $m = 3$ in the limit $h_* \ll h$ (see González et al. 2013). In the limit $h_* \ll h_0$, λ_m does not depend on n. Based on LSA, one can extract a typical timescale for instability development, τ_s (the inverse of the maximum growth rate),

$$\tau_s = \frac{12\gamma\mu}{h_0\kappa^2}\left[\left(\frac{h_*}{h_0}\right)^m m - \left(\frac{h_*}{h_0}\right)^n n\right]^{-2}. \quad 5.$$

Once this expression is used in the case of metal films, one obtains values that are in accordance with the experimental observations, that is, with evolution on the timescale measured by few laser pulses in the experiments conducted by González et al. (2013).

A few comments are in order regarding the extracted form of the disjoining pressure. First, the analysis was carried out using LSA of the LW model. However, since the experimental results that were used in the analysis come from early stages of evolution, before the formation of drops, one expects that the LW model is still valid. For later stages of evolution, LSA could not be expected to be valid anyway. Consistently, González et al. (2013) showed that a proper spatial scaling of the fully developed metal particles with the film thickness cannot be described within LSA. We note that further insights regarding touchdown time could be obtained by considering nonlinear theories (see Williams & Davis 1982). During the final stage of evolution, nonlinear coarsening effects become important, as we discuss later in this section. Second, it was assumed that spinodal instability is dominant. The scaling of the emerging wavelengths with the film thickness suggests that this assumption is reasonable for thin films. For example, in the Cu films the experiments considered, good scaling was found for the films thinner than ≈12 nm; for thicker films, the dispersion of the experimental data was too large to reach a conclusion. Therefore, the mechanism responsible for instability development for thicker metal films still needs to be confirmed. Finally, thermal effects were not taken into account. While the role of the Marangoni effect is unclear (see Seric et al. 2018b), the fact that the material parameters varied with temperature may have influenced the results. However, careful stability analysis with temperature-dependent material parameters, combined with computations of the temperature field, has not yet been carried out, so the relevance of thermal effects remains to be fully understood.

Film thickness studies have revealed that the characteristic length scale of the instability can be related to the film thickness by power laws, thus providing evidence for a spinodal dewetting instability mechanism. A detailed study (González et al. 2013) indicated that a suitable power law for many experiments could be 3/2, while other authors (Krishna et al. 2010) claimed a power of 2, although it is not obvious whether the (more commonly considered) exponent 2 fits the data any better than 3/2. As already discussed, for thicker films, the nucleation mechanism may be dominant for Krishna et al.'s (2010) and González et al.'s (2013) results, and therefore LSA based on spinodal dewetting may not be appropriate.

3.3. Insights from Simulations

The evolution of metal films is very fast and simulations help to bridge between the states of the system that are observable experimentally. However, fully nonlinear simulations are limited, and

only a handful of research papers consider thin film instabilities in the context of liquid metal films on the nanoscale.

From a modeling point of view, the simplest approach is to consider the liquid metal as a Newtonian fluid and to ignore thermal effects, as discussed above. Even for such a simplified setup, three-dimensional simulations are computationally expensive, and it is tempting to use the LW formulation due to reduced complexity and computational time, despite the large contact angles that are relevant to liquid metals on SiO_2 substrates. Such an approach is supported by recent direct comparison of the LW results with the ones obtained via direct numerical simulations of the NS equations (Mahady et al. 2013). Reasonably good agreement of the results even for large contact angles encourages the use of the LW formulation even outside of its strict range of validity. We note that simulations within the LW formulation (albeit in two spatial dimensions) have also been considered for metal bilayers (Khenner et al. 2011), finding interesting core–shell structures that were also found experimentally (McKeown et al. 2015).

Figure 4 shows an example of the results obtained via direct numerical simulations of the NS equation with an additional term modeling liquid–solid interaction forces (Mahady et al. 2016), as discussed in Section 2.4. Here, the film is perturbed by random perturbations of small amplitudes at an initial time and allowed to evolve. The initial stages of evolution are found to be in very good agreement with LSA obtained within the LW formulation, suggesting again that LW is appropriate for consideration of at least the initial stages of instability. After initial breakup and hole formation, the emerging wave numbers decrease at longer timescales, leading to a slow coarsening in the final pattern of drops. This process could be explained as an example of a coupling of absolute instability, responsible for film breakup, and convective instability, responsible for the evolution after breakup. This coarsening effect, which has a different origin than the long-time coarsening due to communication between the drops through the equilibrium film (Glasner & Witelski 2003), is observed after the original net of filaments, formed due to the increase in size of the holes, begins to break up. At this stage, one has a series of filaments with bulges connected by bridges. The bulges do not necessarily remain in place and tend to move closer together. If there is not enough time to break up the remaining bridges, the bulges might coalesce, leading to larger distances between the drops. A fluid model that takes into account the evolution of filaments is more appropriate for understanding this effect than one that is based only on films. Therefore, we postpone the discussion of this problem to Section 4.

Another issue, where some insight can be reached via simulations, involves the influence of thermal effects on the instability development. Fully nonlinear simulations with self-consistent computations of the thermal field are not trivial, in particular due to the fact that the absorption of heat due to a laser pulse depends on (the local value of) the film thickness, which is itself evolving. While a reasonably good approximation (and even exact results) could be obtained in the case of flat static films on infinitely thick substrates (Trice et al. 2007), the situation is more complicated for the case of evolving films of nonuniform thickness. Recent simulations based on the LW formulation (Dong & Kondic 2016) have shown that the model that ignores film evolution leads to inaccurate results, and that including the film evolution may result in an oscillatory Marangoni instability: Essentially, due to the phase lag between the evolution of the temperature field and the film thickness, the out-of-phase Marangoni effect may lead to an oscillatory film evolution, which may be stable or unstable. Such behavior remains to be seen in experiments involving liquid metals. However, more recent works based on volume of fluid simulations have shown that consideration of the full thermal model (with heat diffusion operating in both in-plane and out-of-plane directions) influences the results for thick substrates (see Seric et al. 2018b). Essentially, allowing for heat diffusion in the in-plane direction decreases temperature gradients and reduces the relevance of the Marangoni effect. One could ask whether consideration of stronger source

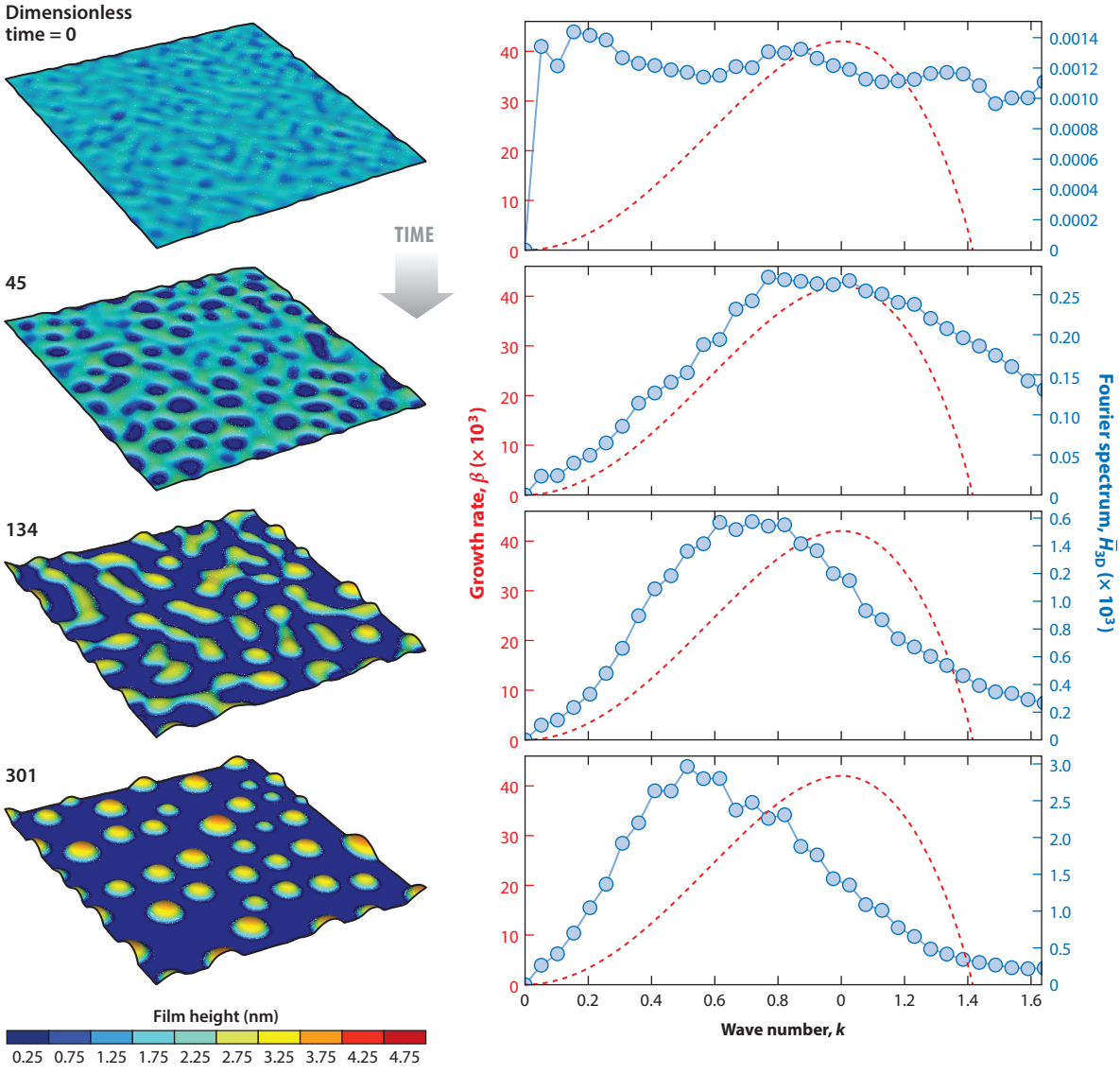

Figure 4

Time evolution of film breakup. The initial condition is a flat film of thickness h_0 and length side L, perturbed by random perturbations. Here h_0 is $L/2 = 4$ nm; the Ohnesorge number Oh is $\mu/\sqrt{\rho\gamma L} = 0.437$, where μ is the viscosity, ρ is the density, and γ is the surface tension (the material parameters for Cu at the melting point were used); and the equilibrium contact angle is approximately 79°. The colors show the logarithm of the height of the interface above the substrate. The plots on the right show associated Fourier spectra H_{3D} (*blue*, right *y*-axes), together with the linear stability analysis predictions for the growth rate β (*red*, left *y*-axes), as a function of wave number k. The times given are in appropriate nondimensional units as defined in the original publication. Note the coarsening effect for later times. Figure adapted from Mahady et al. (2016).

terms, or substrates characterized by different thermal properties, might lead to different results and the oscillatory instability mode discussed above.

Metal film patterning extended into the out-of-plane direction can provide an additional tool to influence thin film instability development, since variable film thickness could introduce regularity

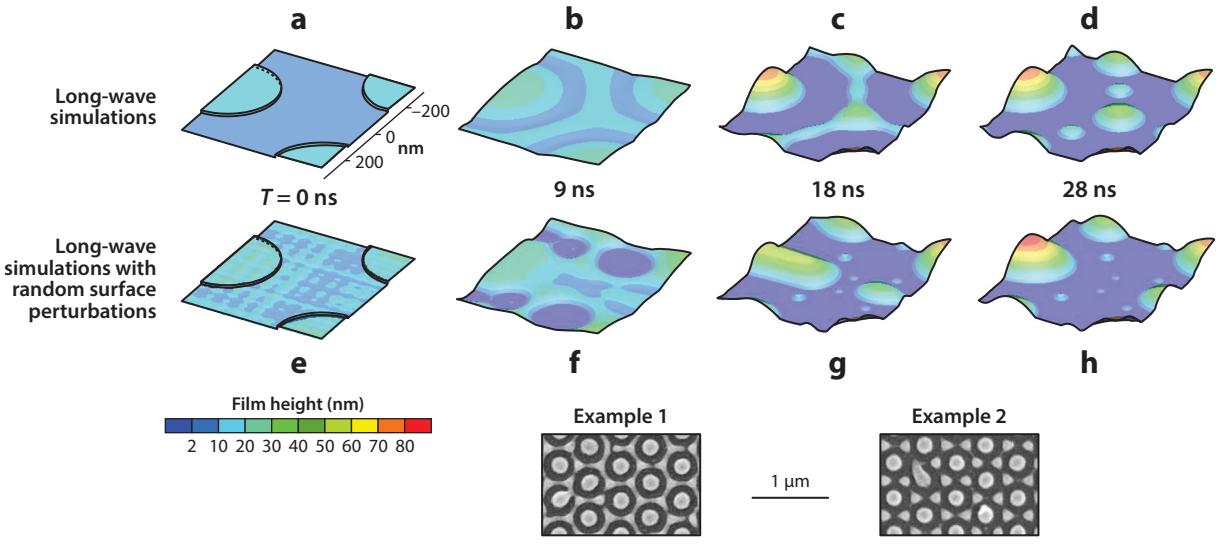

Figure 5

Evolution of an initial Cu pattern formed by thin metal cylinders of 350 nm diameter spaced 600 nm apart in a hexagonal planar array. The cylinders' thickness is 9 nm and they are smoothly covered by a continuous Cu film of thickness 9 nm. (*a–d*) Long-wave simulations showing the complex evolution in response to laser melting. Panels *e–h* show the results of simulations where additional in-plane random surface perturbations have been added. As long as the perturbations are reasonably small, the evolving pattern is only slightly perturbed, indicating that the random perturbations are not dominant. Insets show scanning electron microscopy images for a cylinder diameter of 350 nm and spacing of 500 nm at early stages of the liquid-phase assembly process; these show good agreement with the computed evolution. Figure adapted from Wu et al. (2014).

in the distribution of evolving patterns. For example, PLiD of patterned Ni cylinders on 10-nm-thick films induced the retraction of the cylinder to approximately equal volume hemispheres (Guan et al. 2008). Subsequently, the liquid-phase transport of 30-nm-thick patterned Ni triangles, squares, and circles was studied (Rack et al. 2008). It was shown that enhanced edge retraction occurred via the patterned in-plane radius of curvature and that the retraction velocity slows down as material accumulates, which is a function of the corner angle and is more severe for circles relative to linear edges. **Figure 5** illustrates combined experimental and simulation results from Wu et al. (2014) of the temporal evolution of 350-nm-diameter cylinders with a center-to-center cylinder spacing of 600 nm. Panels *a–d* and *e–h* of **Figure 5** respectively show the evolution without and with the inclusion of random perturbations of 0.5-nm maximum amplitude. Nanoparticle arrays with various primary (positioned in a cylinder pattern) and highly organized secondary and tertiary (inter-cylinder area) particles were found.

3.4. Stochastic Effects

Most of the studies carried out so far have been deterministic, with stochastic effects included only at the initial time by randomly perturbing the initial condition. Fully stochastic models have also been considered within the context of metal films (see Nesic et al. 2015 and Diez et al. 2016). The superposition of white noise in time and colored noise in space might lead to changes in the power spectra of the modes. The results show that the final number of drops is reduced when spatially correlated noise is considered. Moreover, the spatial noise tends to be more correlated as one moves to the center of the laser spot, where the liquid lifetimes are larger and the instability

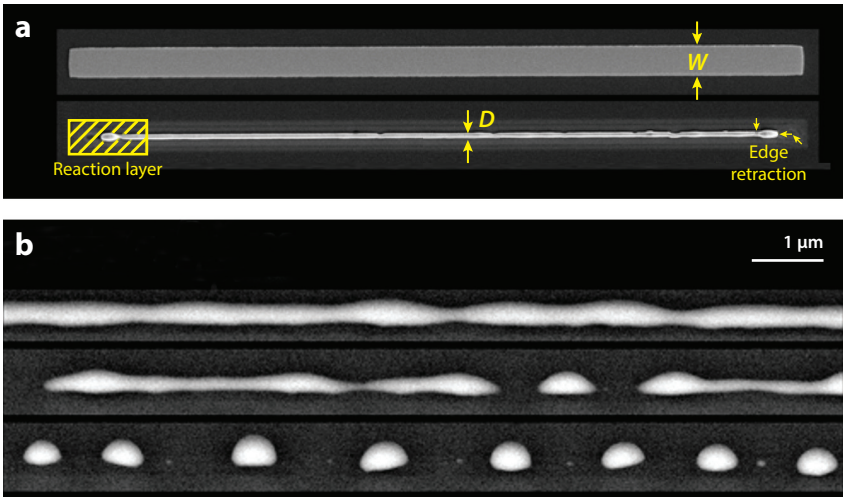

Figure 6

(*a*) Scanning electron microscopy image of a Ni thin film strip following electron beam lithography. The thin film strip dimensions are $h_0 = 23 \pm 1.2$ nm, $w = 2.05$ μm $\pm$ 18 nm, and $L = 50$ μm. The strip transforms rapidly by fluid retraction into a rounded filament upon pulsed-laser melting with an average diameter of D. (*b*) Time evolution of the filament. These images were acquired at an angle with respect to the Si substrate. The tilted images reveal the wetting profile at the metal–substrate interface following metal solidification. The scale bar has been set to equal the fastest growing mode as predicted by the Rayleigh–Plateau instability of a liquid jet. The nanoparticle spacing reflects this value. Figure adapted from Fowlkes et al. (2011).

pattern observed corresponds to later stages of the instability. While the colored spatial thermal noise may alter the spectral distribution shape, the wave number of its maximum for late times is close to the LSA deterministic value. Therefore, the typical lengths of the patterns in advanced stages of the instability are weakly dependent on stochasticity.

4. FILAMENTS AND RELATED PROBLEMS

4.1. Filament Instability and Self-Assembly

Figure 6 illustrates another basic geometry that has been used in experiments involving liquid metals. Essentially, a thin flat filament (of rectangular cross section) is deposited on a substrate; then, upon exposure to laser irradiation and melting, the filament's cross section transforms on a fast timescale to a semicircular shape. The instability evolution that results for this pseudo-one-dimensional filament is the main focus of this section.

Figure 6 shows that the semicircular liquid metal filaments break up into drops that after solidification remain on the substrate as metal particles. To understand the instability mechanism, one is tempted to think in terms of an RP instability involving the breakup of a free-standing cylindrical jet. This paradigm has been widely applied, particularly in the materials science literature. However, it is important to point out that there are significant differences between the instability mechanisms of a free jet and one that is placed on a substrate where wetting and dewetting processes are crucial. The interaction of a fluid filament with a substrate may play a significant role, and as discussed in a more general context (Diez et al. 2009), the interpretation of the results depends strongly on how one defines the equivalent RP jet that corresponds to the filament considered. Using the parameters that are typical for nanoscale liquid metal experiments, one therefore

finds the relevant timescale, $\tau_s \approx 10$ ns, to be comparable to the duration of a laser pulse. Consistently, one finds that the instabilities develop in physical experiments during one to two laser pulses.

Another feature illustrated in **Figure 6** as well as in many other experiments is the fact that the filaments are of finite length and, as a consequence, are prone to a pearling instability (Powers & Goldstein 1997, Powers et al. 1998), in contrast to a RP-type instability, which assumes that the perturbation grows all along an infinite filament. The relevance of the pearling process depends on the filament aspect ratio, but it is clear that pearling plays a significant role in many experiments (e.g., Kondic et al. 2009, Cuellar et al. 2017). When the filaments are short enough (Cuellar et al. 2017), the pearling process yields outcomes (such as the distance between the drops) that are different from those predicted by RP. However, in other cases (Kondic et al. 2009), the experimental and computational final outcome does not show any significant difference, probably due to the length and aspect ratios considered.

While filaments always have ends, consideration of a ring geometry removes their presence, and one could ask whether thin metal rings would evolve in any different manner compared to finite-length filaments. Such a study was carried out using Cu rings of various widths and thicknesses on SiO_2 substrates (Wu et al. 2010). While for narrow rings the results were similar to filaments, for wider rings, the experiments (as well as simulations) uncovered an interplay between (axial) filament breakup and (radial) breakup of a finite-length thin film (Wu et al. 2011b). **Figure 7**

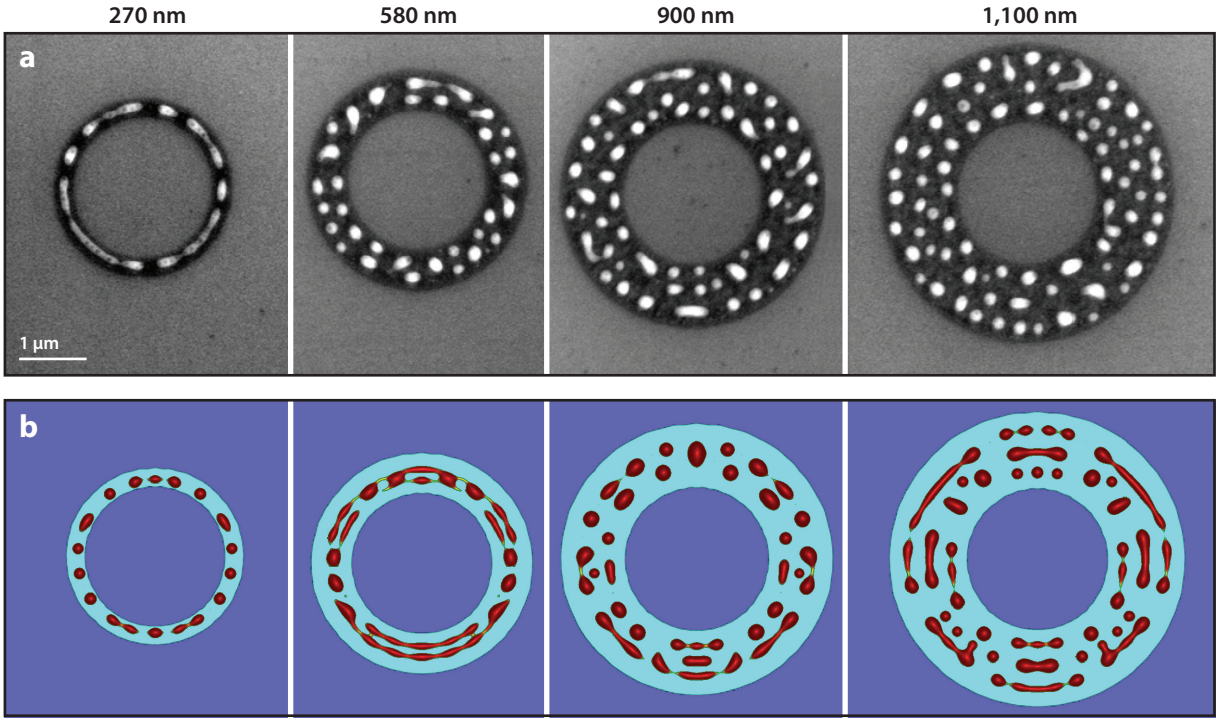

Figure 7

(*a*) Scanning electron micrographs of approximately 8-nm-thick metal rings of various widths following pulsed laser exposure. (*b*) Simulations (long-wave based) of the same geometry. The figure illustrates that as the width of the ring increases, the ring transitions from a Rayleigh–Plateau-type instability in the azimuthal direction to a different regime such that both thin film instability (in the radial direction) and Rayleigh–Plateau-type instability are operative. Figure adapted from Wu et al. (2011b).

shows surprisingly good agreement between experiments and simulations (Wu et al. 2011b). Since the simulations were carried out within the LW formulation, here is another example of the use of the LW approach to provide reasonable results outside of its range of validity. Similar results for (narrow) ring breakup were obtained using MD simulations (Nguyen et al. 2012). From a continuum fluid mechanical point of view, the ring breakup process is complicated due to various issues that have not been considered in the LW simulation mentioned above, such as contact angle hysteresis (Gonzalez et al. 2013). Not only for liquid metals but in general, it is still a challenge to model in a consistent manner time-dependent evolution involving contact angle hysteresis.

An additional insight into various instability mechanisms can be reached by considering short filaments and asking what is the transition length scale for collapse to a single drop versus breakup into two drops. An analytical model based on Driessen et al. (2013) for viscous breakup and a modified model for viscoinertial breakup was applied to understand this process. For the considered geometry, it turns out that a viscoinertial model best fits the data, as expected due to low Ohnesorge number (<0.2). Volume of fluid simulations have revealed that the resolidification of the receding filament mutes some of the inertial contributions, leading to longer critical lengths (Hartnett et al. 2015).

4.2. Directed Assembly

The idea of directed assembly is attractive for improving control of the size and spacing of nanoparticles (Hughes et al. 2017). The corresponding setup can be established via synthetic perturbations added to deposited filaments (Fowlkes et al. 2011). Varicose sinusoidal patterns with various wavelengths and amplitudes were patterned onto the line edges and subsequently liquefied via laser irradiation. Both stable and unstable wavelengths were investigated, with stability boundaries determined approximately by the RP-type instability. **Figure 8** shows a few examples of the results. It turns out that with very high fidelity, nanoparticle size and spacing can be achieved via imposed perturbations, as long as these belong to the unstable part of the spectrum. Interestingly, MD simulations of synthetic perturbations at the nanometer length scale also demonstrated controlled assembly, although stochastic effects at the considered length scale are more significant (Fowlkes et al. 2012a). Another finding reported by Fowlkes et al. (2014) was the formation of hierarchical nanoparticle arrays, where secondary and tertiary satellite nanoparticles were observed. An approximately order-of-magnitude change in the particle size occurs in the transitions from primary to secondary and secondary to tertiary nanoparticles, with sizes and spacing controlled by the original pattern.

Conveniently, standard lithographic techniques can be used to pattern the relevant metal films of interest. Therefore, one could produce initial conditions that may be difficult to obtain in other fluid-based systems. One example of such a setup was considered recently in experiments (Roberts et al. 2013) and simulations (Mahady et al. 2015b). In these works, instead of sinusoidal patterns, square wave patterns were imposed. It turns out that for sufficiently large perturbation amplitudes, a variety of patterns are possible, ranging from high fidelity to essentially a disordered array of drops. Volume of fluid–based simulations (Mahady et al. 2015b), which analyzed in detail the evolution of imposed patterns, showed that repeated breakup and merging of perturbations and the main body of the filament could lead to a complex set of emerging patterns. Perhaps unexpectedly, the results show that a regular set of drops can be formed from an initial imposed perturbation whose characteristic length would be stable according to LSA predictions.

Another recent direction that involved combined experimental, modeling, and computational efforts involves manipulating the surface energy to invoke solutal Marangoni forces, in order to facilitate the assembly of nanoparticle arrays (Hartnett et al. 2017). Specifically, patterned Ni strips

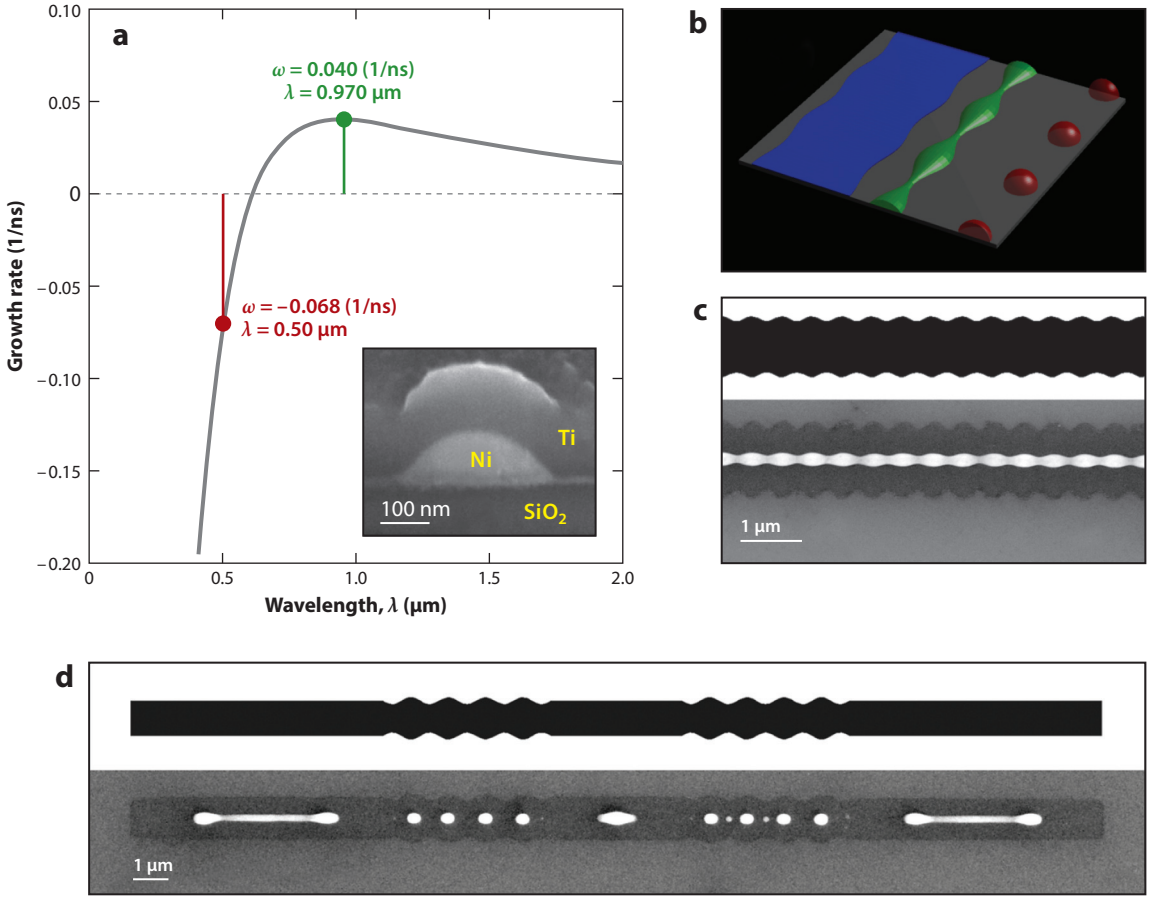

Figure 8

(*a*) An example of a dispersion curve showing the growth rate relevant to typical experiments with liquid metal filaments (see Fowlkes et al. 2012b). The broad spectrum ensures that multiple modes influence the filament breakup yielding a variable droplet spacing. The green and red dots correspond to imposed perturbation wavelengths, as illustrated in the other panels. (*b*) Introducing a perturbation (*blue*) with nanoscale amplitude imposes order, acting essentially as a noise filter (*green*) leading to drops (*red*). (*c*) Stable decaying modes may also be imposed by an initial modulated configuration. These filaments eventually break up due to natural noise, but on longer timescales. (*d*) Straight edges and unstable modes may be combined using lithography and pulsed-laser-induced dewetting to generate ordered particles and filaments. Figure adapted from Fowlkes et al. (2012b).

were coated with a thin Cu pattern to induce a surface energy gradient, as the Cu and Ni surface energies at the nickel melting temperature are 1.24 and 1.77 N/m, respectively. The Cu patterns were set equal to half of the patterned wavelength, and both stable and unstable modes expected from the RP-type instability were explored. The surface energy gradient indeed induced flow toward the Ni surface region as evidenced by the resultant nanoparticle placement for unstable modes after the PLiD.

An alternative approach to directing instability is to consider a fully two-dimensional setup and then, instead of a single filament, focus on a rectangular mesh of filaments. Studies show that besides the drops at the nodes, the number of drops per side of the rectangle can be predicted by considering the process of retraction and breakup of finite filaments (Cuellar et al. 2017, 2018). The dewetting process along the filament at its ends is like a snowplow that leads to the formation

of a bulge at their tips, which is concomitant with a wetting process in the transverse direction of the original filament. At a critical point, the bulges have reached a quasi-static equilibrium with the rest of the straight filament. However, this equilibrium is not stable and a small perturbation leads to necks. Due to the different curvatures (longitudinal and transversal) at the bridge center and those at its ends, a pressure difference is established, and as a consequence, Stokes flow depletes the neck region leading to an eventual breakup. The two characteristic distances from unperturbed regions, both from the bulge and the filament, can be obtained using a simple fluid mechanical balance (Cuellar et al. 2017). The process is repeated sequentially in the remaining filaments after the breakup of the bulges forming drops until the final pattern of particles is obtained. The estimates based on detailed analysis of this process of the distances between drops and the final number of particles show a remarkable agreement with experiments carried out with Cu rectangular grids (Cuellar et al. 2018).

Beyond lithographic patterning, shaping the laser beam has also been used for assembling nanoparticles. For instance, a donut-shaped laser beam with an outer radius of ∼5 μm was used to induce a thermocapillary flow and generate ∼0.5-μm-diameter Si hemispherical particles on demand. Kuchmizhak et al. (2016) generated various nanodrops, nanorods, nanorings, and nanocrown morphologies via controlled fluid transport and rapid resolidification. Furthermore, PLiD and breakup via the filament instability of randomly aligned Ag nanowires and Au-coated Ag nanowires have been explored for producing nanoparticle arrays for plasmonic applications (H. Oh et al. 2018). Of course, these more complicated setups require additional modeling and simulations to be fully understood and utilized.

5. OPEN PROBLEMS AND FUTURE DIRECTIONS

The basic principles of liquid metal film dewetting are reasonably well understood, yet there remain many aspects requiring a more thorough investigation. These aspects typically involve configurations where multiphysics effects become relevant. While from a theoretical point of view there are many issues that require and careful modeling and computation (such as stochastic effects, phase change, and careful coupling of thermal and fluid mechanical aspects), from an application point of view one could isolate in particular three aspects that we recommend for consideration: (*a*) templated substrates leading to coupling of thermal effects with fluid mechanical ones; (*b*) bimetalic and miscible configurations; and (*c*) immiscible alloys where competition between chemical and fluid mechanical instabilities becomes relevant.

Regarding templated thermal transport, one possibility is to use structured substrates to dictate thermal gradients and subsequently program evolving instabilities. For instance, one could pattern planar disparate thermal conductivity substrate materials (e.g., Si and SiO_2 with thermal conductivities of 130 and 1.4 W/mK, respectively). The question is to what degree such substrates could be used to guide the instability development and produce a desired set of patterns. From a modeling point of view, such a setup would require much more careful modeling of the thermal effects compared to what has been achieved so far.

Regarding the second direction, we note that McKeown et al. (2015) considered bi-metal Co–Cu thin films using a technique similar to that used by McKeown et al. (2012). These films are interesting because the metals are miscible when both are in their liquid phase but have limited miscibility when Cu is liquid and Co is solid. The later state may happen when the laser fluence is low enough, since the Cu melting temperature is ∼500 K less than that of Co. To study whether the melting of two mixed metals will yield core–shell-type geometries, Dai et al. (2017) studied the effect of the substrate on the morphology of a cladded Cu–Fe molten metal coating. Inclusion of relevant physics in appropriate models is complicated, since the process of core–shell formation

involves variable (material-dependent) metal/substrate interaction energies. We note that some progress in modeling such systems has been reported recently (Khenner et al. 2011). In addition to immiscible systems, liquid-phase dewetting of miscible/soluble alloys has also been considered experimentally (Y. Oh et al. 2018; Beliatis et al. 2011; Wu et al. 2011a, 2016; Censabella et al. 2018). The relevance of these systems comes from the fact that they have both complete solid- and liquid-phase solubility, so the plasmonic resonance energy can be tuned via both particle size and composition. Theoretical understanding of fluid mechanical aspects of such setups remains to be developed.

Considering now immiscible alloys, note that when a binary alloy is below its critical temperature (Bray 2002), the mixed state is energetically unfavorable, and the system spontaneously phase separates and forms domains rich in one of the fluid components. If attention is restricted to the case where both elements in the alloy experience the same interaction with the substrate and free surface, the so called H-model (based on the coupled NS Cahn–Hilliard equations) is usually employed (Lowengrub & Truskinovsky 1998, Thiele et al. 2007). Such modeling has to be completed by boundary conditions at both the solid substrate and the free surface, since it allows one to describe the creation and evolution of internal diffuse interfaces within the film. The interaction between these internal and the external interfaces is governed by a solutal Marangoni effect, which results in an additional driving force of the evolution. Thus, the model highlights the effect of the dynamical back reaction of concentration gradients on the flow, a useful feature in applications where control of phase separation is required. To understand the influence of thin film geometry on phase separation, one approach is to use the LW model (Náraigh & Thiffeault 2010). Since this simplification suppresses the out-of-plane variations in the concentration field, it is limited to the case where the binary fluid components interact identically with the substrate and free surface. However, the model is able to give an accurate description of the surface roughening arising from liquid–solid interaction forces. More detailed models based on this approach, involving different boundary conditions that better reflect wetting behavior (Das et al. 2006) and a concentration-dependent Hamaker coefficient, can capture a wider range of thin film behavior. However, we still lack an appropriate formulation of such a model for considering immiscible alloys on nanoscale.

While multimetal investigations have been explored in the form of both codeposited alloys or multilayer films, little is understood regarding the competition between the chemical instabilities in, for instance, immiscible systems relative to the concurrent instabilities caused by fluid mechanics. Perhaps exploiting competing chemical and hydrodynamic instabilities could be a route for better assembly control for multimaterial/multifunctional nanoparticles. In particular, the relative importance of the phenomena related to phase separation and to fluid mechanical instabilities remains an open question. One important aspect of what remains to be done is to develop more accurate models and simulations that would self-consistently include the outlined effects. Development of such models and simulations, as well as supporting experiments, remains as a challenge.

DISCLOSURE STATEMENT

The authors are not aware of any biases that might be perceived as affecting the objectivity of this review.

ACKNOWLEDGMENTS

L.K. acknowledges support by NSF CBET-1604351 and DMS-1815613. A.G.G. and J.A.D. are CONICET researchers and acknowledge support from Agencia Nacional de Promoción

Científica y Tecnológica (ANPCyT, Argentina) with grant number PICT 1067/2016. P.R. acknowledges support from NSF CBET-1603780, and J.D.F. acknowledges support from the Center for Nanophase Materials Sciences, which is a DOE Office of Science User Facility.

LITERATURE CITED

Afkhami S, Kondic L. 2013. Numerical simulation of ejected molten metal nanoparticles liquified by laser irradiation: interplay of geometry and dewetting. *Phys. Rev. Lett.* 111:034501

Afkhami S, Zaleski S, Bussmann M. 2009. A mesh-dependent model for applying dynamic contact angles to VOF simulations. *J. Comput. Phys.* 228:5370–89

Ahmmed MS, Huda N. 2018. A detailed study on melting dynamics influenced by the pulse laser-induced transient heating. *Thermal Sci. Eng. Prog.* 7:54–60

Ajaev VS. 2013. Instability and rupture of thin liquid films on solid substrates. *Interfacial Phenom. Heat Transf.* 1:81–92

Ajaev VS, Willis DA. 2003. Thermocapillary flow and rupture in films of molten metal on a substrate. *Phys. Fluids* 15:3144–50

Andreotti B, Snoeijer JH. 2020. Statics and dynamics of soft wetting. *Annu. Rev. Fluid Mech.* 52:285–308

Arnold W, Hunklinger S, Dransfeld K. 1979. Influence of optical absorption on the van der Waals interaction between solids. *Phys. Rev. B* 19:6049–56

Atena A, Khenner M. 2009. Thermocapillary effects in driven dewetting and self assembly of pulsed-laser-irradiated metallic films. *Phys. Rev. B* 80:075402

Bao Y, Guérout R, Lussange J, Lambrecht A, Cirelli RA, et al. 2010. Casimir force on a surface with shallow nanoscale corrugations: geometry and finite conductivity effects. *Phys. Rev. Lett.* 105:250402

Batič BŠ, Verbovšek T, Šetina J. 2017. Decomposition of thin Au films on flat and structured Si substrate by annealing. *Vacuum* 138:134–38

Becker J, Grün G, Seemann R, Mantz H, Jacobs K, et al. 2003. Complex dewetting scenarios captured by thin-film models. *Nat. Mat.* 2:59–63

Beliatis MJ, Henley SJ, Silva SRP. 2011. Engineering the plasmon resonance of large area bimetallic nanoparticle films by laser nanostructuring for chemical sensors. *Opt. Lett.* 36:1362–64

Bestehorn M, Merkt D. 2006. Regular surface patterns on Rayleigh-Taylor unstable evaporating films heated from below. *Phys. Rev. Lett.* 97:12780

Bischof J, Scherer D, Herminghaus S, Leiderer P. 1996. Dewetting modes of thin metallic films: nucleation of holes and spinodal dewetting. *Phys. Rev. Lett.* 77:1536–39

Bonn D, Eggers J, Indekeu J, Meunier J, Rolley E. 2009. Wetting and spreading. *Rev. Mod. Phys.* 81:739–805

Bray AJ. 2002. Theory of phase-ordering kinetics. *Adv. Phys.* 51:481–87

Briant AJ, Wagner AJ, Yeomans JM. 2004. Lattice Boltzmann simulations of contact line motion. I. Liquid-gas systems. *Phys. Rev. E* 69:031602

Burelbach JP, Bankoff SG, Davis SH. 1988. Nonlinear stability of evaporating/condensing liquid films. *J. Fluid Mech.* 195:463–94

Butt HJ, Kappl M. 2010. Surface and Interfacial Forces. Weinheim, Ger.: Wiley-VCH Verlag

Censabella M, Ruffino F, Zimbone M, Bruno E, Grimaldi MG. 2018. Self-organization based fabrication of bimetallic PtPd nanoparticles on transparent conductive oxide substrates. *Phys. Status Solidi A* 215:1700524

Chan HB, Bao Y, Zou J, Cirelli RA, Klemens F, et al. 2008. Measurement of the Casimir force between a gold sphere and a silicon surface with nanoscale trench arrays. *Phys. Rev. Lett.* 101:030401

Chen F, Klimchitskaya GL, Mostepanenko VM, Mohideen U. 2007. Control of the Casimir force by the modification of dielectric properties with light. *Phys. Rev. B* 76:035338

Colinet P, Legros JC, Velarde MG. 2001. Nonlinear Dynamics of Surface-Tension-Driven Instabilities. Berlin: Wiley-VCH

Craster R, Matar O. 2009. Dynamics and stability of thin liquid films. *Rev. Mod. Phys.* 81:1131–98

Cuellar I, Ravazzoli PD, Diez JA, González AG. 2017. Drop pattern resulting from the breakup of a bidimensional grid of liquid filaments. *Phys. Fluids* 29:102103

Cuellar I, Ravazzoli PD, Diez JA, González AG, Roberts NA, et al. 2018. Self-assembly of a drop pattern from a two-dimensional grid of nanometric metallic filaments. *Phys. Rev. E* 98:043101

Dai X, Zhou S, Wang M, Lei J, Xie M, et al. 2017. Effect of substrate types on the microstructure and properties of Cu65Fe35 composite coatings by laser induction hybrid cladding. *J. Alloys Compd.* 722:173–82

Das SK, Puri S, Horbach J, Binder K. 2006. Spinodal decomposition in thin films: molecular-dynamics simulations of a binary Lennard-Jones fluid mixture. *Phys. Rev. E* 73:031604

Derjaguin B, Leonov L, Roldughin V. 1985. Disjoining pressure in liquid metallic films. *J. Colloid Interface Sci.* 108:207–14

Diez JA, González AG, Fernández R. 2016. Metallic-thin-film instability with spatially correlated thermal noise. *Phys. Rev. E* 93:013120

Diez JA, González AG, Kondic L. 2009. On the breakup of fluid rivulets. *Phys. Fluids* 21:082105

Diez JA, Kondic L. 2007. On the breakup of fluid films of finite and infinite extent. *Phys. Fluids* 19:072107

Dong N, Kondic L. 2016. Instability of nanometric fluid films on a thermally conductive substrate. *Phys. Rev. Fluids* 1:063901

Driessen T, Jeurissen R, Wijshoff H, Toschi F, Lohse D. 2013. Stability of viscous long liquid filaments. *Phys. Fluids* 25:062109

Favazza C, Kalyanaraman R, Sureshkumar R. 2006a. Robust nanopatterning by laser-induced dewetting of metal nanofilms. *Nanotechnology* 17:4229–34

Favazza C, Trice J, Krishna H, Kalyanaraman R, Sureshkumar R. 2006b. Laser-induced short- and long-range orderings of Co nanoparticles on SiO_2. *Appl. Phys. Lett.* 88:153118

Fetzer R, Jacobs K, Münch A, Wagner B, Witelski TP. 2005. New slip regimes and the shape of dewetting thin liquid films. *Phys. Rev. Lett.* 95:127801

Font F, Afkhami S, Kondic L. 2017. Substrate melting during laser heating of nanoscale metal films. *Int. J. Heat Mass Transf.* 113:237–45

Fowlkes JD, Horton S, Fuentes-Cabrera M, Rack PD. 2012a. Signatures of the Rayleigh-Plateau instability revealed by imposing synthetic perturbations on nanometer-sized liquid metals on substrates. *Angew. Chem. Int. Ed.* 51:8768–72

Fowlkes JD, Kondic L, Diez JA, Gonzalez AG, Wu Y, et al. 2012b. Parallel assembly of particles and wires on substrates by dictating instability evolution in liquid metal films. *Nanoscale* 4:7376–82

Fowlkes JD, Kondic L, Diez JA, Rack PD. 2011. Self-assembly versus directed assembly of nanoparticles via pulsed laser induced dewetting of patterned metal films. *Nano Lett.* 11:2478–85

Fowlkes JD, Roberts NA, Wu Y, Diez JA, González AG, et al. 2014. Hierarchical nanoparticle ensembles synthesized by liquid phase directed self-assembly. *Nano Lett.* 14:774–82

Francois MM, Cummins SJ, Dendy ED, Kothe DB, Sicilian JM, Williams MW. 2006. A balanced-force algorithm for continuous and sharp interfacial surface tension models within a volume tracking framework. *J. Comput. Phys.* 213:141–73

Fuentes-Cabrera M, Rhodes BH, Baskes M, Terrones H, Fowlkes J, et al. 2011a. Controlling the velocity of jumping nanodroplets via their initial shape and temperature. *ACS Nano* 5:7130–36

Fuentes-Cabrera M, Rhodes BH, Fowlkes JD, López-Benzanilla A, Terrones H, et al. 2011b. Molecular dynamics study of the dewetting of copper on graphite and graphene: implications for nanoscale self-assembly. *Phys. Rev. E* 83:041603

Garcia H, Sachan R, Kalyanaraman R. 2012. Plasmon properties of Co-Ag nanocomposites within the mean-field approximation. *Plasmonics* 7:137–41

Garnett EC, Brongersma ML, Cui Y, McGehee MD. 2011. Nanowire solar cells. *Annu. Rev. Mat. Res.* 41:269–95

Glasner KB, Witelski TP. 2003. Coarsening dynamics of dewetting films. *Phys. Rev. E* 67:016302

Gonzalez AG, Diez JA, Kondic L. 2013. Stability of a liquid ring on a substrate. *J. Fluid Mech.* 718:246–79

González AG, Diez JA, Sellier M. 2016. Inertial and dimensional effects on the instability of a thin film. *J. Fluid Mech.* 787:449–73

González AG, Diez JA, Wu Y, Fowlkes JD, Rack PD, Kondic L. 2013. Instability of liquid Cu films on a SiO_2 substrate. *Langmuir* 29:9378–87

Guan YF, Pearce RC, Melechko AV, Hensley DK, Simpson ML, Rack PD. 2008. Pulsed laser dewetting of nickel catalyst for carbon nanofiber growth. *Nanotechnology* 19:235604
Gurevich EL. 2011. Self-organized nanopatterns in thin layers of superheated liquid metals. *Phys. Rev. E* 83:031604
Habenicht A, Olapinski M, Burmeister F, Leiderer P, Boneberg J. 2005. Jumping nanodroplets. *Science* 309:2043–45
Hartnett CA, Mahady K, Fowlkes JD, Afkhami S, Kondic L, Rack PD. 2015. Instability of nano- and microscale liquid metal filaments: transition from single droplet collapse to multidroplet breakup. *Langmuir* 31:13609–17
Hartnett CA, Seric I, Mahady K, Kondic L, Afkhami S, et al. 2017. Exploiting the Marangoni effect to initiate instabilities and direct the assembly of liquid metal filaments. *Langmuir* 33:8123–28
Herminghaus S, Jacobs K, Mecke K, Bischof J, Fery A, et al. 1998. Spinodal dewetting in liquid crystal and liquid metal films. *Science* 282:916–19
Hughes RA, Menumerov E, Neretina S. 2017. When lithography meets self-assembly: a review of recent advances in the directed assembly of complex metal nanostructures on planar and textured surfaces. *Nanotechnology* 28:282002
Inui N. 2007. Change in the Casimir force between semiconductive bodies by irradiation. *J. Phys. Conf. Ser.* 89:012018
Israelachvili JN. 1992. Intermolecular and Surface Forces. New York: Academic. 2nd ed.
Jacobs K, Seemann R, Herminghaus S. 2008. Stability and dewetting of thin liquid films. In *Polymer Thin Films*, ed. OKC Tsui, TP Russell, pp. 243–65. Hackensack, NJ: World Sci.
Jacqmin J. 2000. Contact-line dynamics of a diffuse fluid interface. *J. Fluid Mech.* 402:57–88
Jacqmin J. 2004. Onset of wetting failure in liquid–liquid systems. *J. Fluid Mech.* 517:209–28
Khenner M, Yadavali S, Kalyanaraman R. 2011. Formation of organized nanostructures from unstable bilayers of thin metallic liquids. *Phys. Fluids* 23:122105
Klimchitskaya GL, Mohideen U, Mostepanenko VM. 2009. The Casimir force between real materials: experiment and theory. *Rev. Mod. Phys.* 81:1827–85
Kondic L, Diez JA, Rack PD, Guan Y, Fowlkes JD. 2009. Nanoparticle assembly via the dewetting of patterned thin metal lines: understanding the instability mechanisms. *Phys. Rev. E* 79:026302
Krishna H, Sachan R, Strader J, Favazza C, Khenner M, Kalyanaraman R. 2010. Thickness-dependent spontaneous dewetting morphology of ultrathin Ag films. *Nanotechnology* 21:155601
Krishna H, Shirato N, Favazza C, Kalyanaraman R. 2009. Energy driven self-organization in nanoscale metallic liquid films. *Phys. Chem. Chem. Phys.* 11:8136–43
Krishna H, Shirato N, Yadavali S, Sachan R, Strader J, Kalyanaraman R. 2011. Self–organization of nanoscale multilayer liquid metal films: experiment and theory. *ACS Nano* 5:470–76
Kuchmizhak A, Gurbatov S, Vitrik O, Kulchin Y, Milichko V, et al. 2016. Ion-beam assisted laser fabrication of sensing plasmonic nanostructures. *Sci. Rep.* 6:19410
Lam MAYH, Cummings LJ, Kondic L. 2018a. Computing dynamics of thin films via large scale GPU-based simulations. *J. Comput. Phys. X* 1:100001
Lam MAYH, Cummings LJ, Kondic L. 2018b. Stability of thin fluid films characterised by a complex form of effective disjoining pressure. *J. Fluid Mech.* 841:925–61
Landau LD, Lifshitz E. 1980. Statistical Physics, Part 2. Oxford: Pergamon
Lee T, Liu L. 2010. Lattice Boltzmann simulations of micron-scale drop impact on dry surfaces. *J. Comput. Phys.* 229:8045–63
Lorenz P, Klöppel M, Frost F, Ehrhardt M, Zimmer K, Li P. 2013. Laser-induced circular nanostructures in fused silica assisted by a self-assembling chromium layer. *Appl. Surface Sci.* 280:933–39
Lowengrub J, Truskinovsky L. 1998. Quasi-incompressible Cahn–Hilliard fluids and topological transitions. *Proc. R. Soc. Lond. A* 454:2617–54
Mahady K, Afkhami S, Diez J, Kondic L. 2013. Comparison of Navier–Stokes simulations with long-wave theory: study of wetting and dewetting. *Phys. Fluids* 25:112103
Mahady K, Afkhami S, Kondic L. 2015a. A volume of fluid method for simulating fluid/fluid interfaces in contact with solid boundaries. *J. Comput. Phys.* 294:243–57

Mahady K, Afkhami S, Kondic L. 2015b. On the influence of initial geometry on the evolution of fluid filaments. *Phys. Fluids* 27:092104
Mahady K, Afkhami S, Kondic L. 2016. A numerical approach for the direct computation of flows including fluid-solid interaction: modeling contact angle, film rupture, and dewetting. *Phys. Fluids* 28:062002
Makarov SV, Milichko VA, Mukhin IS, Shishkin II, Zuev DA, et al. 2016. Controllable femtosecond laser-induced dewetting for plasmonic applications. *Laser Photonics Rev.* 10:91–99
McKeown JT, Roberts NA, Fowlkes JD, Wu Y, LaGrange T, et al. 2012. Real-time observation of nanosecond liquid-phase assembly of nickel nanoparticles via pulsed-laser heating. *Langmuir* 28:17168–75
McKeown JT, Wu Y, Fowlkes JD, Rack PD, Campbell GH. 2015. Simultaneous in-situ synthesis and characterization of Co@Cu core-shell nanoparticle arrays. *Adv. Mater.* 27(6):1060–65
Mitlin VS. 1994. On dewetting conditions. *Colloids Surf.* 89:97–101
Mitlin VS. 2000. Dewetting revisited: new asymtotics of the film stability diagram and the metastable regime of nucleation and growth of dry zones. *J. Colloid Interface Sci.* 227:371–79
Mokkapati S, Catchpole KR. 2012. Nanophotonic light trapping in solar cells. *J. Appl. Phys.* 112:101101
Münch A, Wagner B. 2005. Contact-line instability of dewetting thin films. *Physica D* 209:178–90
Náraigh LO, Thiffeault JL. 2010. Nonlinear dynamics of phase separation in thin films. *Nonlinearity* 23:1559–83
Nesic S, Cuerno R, Moro E, Kondic L. 2015. Dynamics of thin fluid films controlled by thermal fluctuations. *Phys. Rev. E* 92:061002(R)
Nguyen TD, Fuentes-Cabrera M, Fowlkes JD, Diez JA, González AG, et al. 2012. Competition between collapse and breakup in nanometer-sized thin rings using molecular dynamics and continuum modeling. *Langmuir* 28:13960–67
Nguyen TD, Fuentes-Cabrera M, Fowlkes JD, Rack P. 2014. Coexistence of spinodal instability and thermal nucleation in thin-film rupture: insights from molecular levels. *Phys. Rev. E* 89:032403
Oh H, Lee J, Lee M. 2018. Transformation of silver nanowires into nanoparticles by Rayleigh instability: comparison between laser irradiation and heat treatment. *Appl. Surf. Sci.* 427:65–73
Oh Y, Lee J, Lee M. 2018. Fabrication of Ag-Au bimetallic nanoparticles by laser-induced dewetting of bilayer films. *Appl. Surf. Sci.* 434:1293–99
Oron A, Davis SH, Bankoff SG. 1997. Long-scale evolution of thin liquid films. *Rev. Mod. Phys.* 69:931–80
Parsegian VA. 2006. Van der Waals Forces. Cambridge, UK: Cambridge Univ. Press
Popinet S. 2009. An accurate adaptive solver for surface-tension-driven interfacial flows. *J. Comput. Phys.* 228:5838–66
Powers TR, Goldstein RE. 1997. Pearling and pinching: propagation of Rayleigh instabilities. *Phys. Rev. Lett.* 78:2555–58
Powers TR, Zhang D, Goldstein RE, Stone HA. 1998. Propagation of a topological transition: the Rayleigh instability. *Phys. Fluids* 10:1052–57
Rack PD, Guan Y, Fowlkes JD, Melechko AV, Simpson ML. 2008. Pulsed laser dewetting of patterned thin metal films: a means of directed assembly. *Appl. Phys. Lett.* 92:223108
Ratautas K, Gedvilas M, Raciukaitis G, Grigonis A. 2012. Nanoparticle formation after nanosecond-laser irradiation of thin gold films. *J. Appl. Phys.* 112:013108
Reinhardt H, Kim HC, Pietzonka C. 2013. Self-organization of multifunctional surfaces—the fingerprints on a complex system. *Adv. Mat.* 25:3313–18
Renardy Y, Renardy M. 2002. PROST: a parabolic reconstruction of surface tension for the volume-of-fluid method. *J. Comput. Phys.* 183:400–21
Roberts NA, Fowlkes JD, Mahady K, Afkhami S, Kondic L, Rack P. 2013. Directed assembly of one- and two-dimensional nanoparticle arrays from pulsed laser induced dewetting of square waveforms. *ACS Appl. Mater. Interfaces* 5:4450–56
Ross FM. 2010. Controlling nanowire structures through real time growth studies. *Rep. Prog. Phys.* 73:114501
Ruffino F, Gentile A, Zimbone M, Piccitto G, Reitano R, Grimaldi MG. 2016. Size-selected Au nanoparticles on FTO substrate: controlled synthesis by the Rayleigh-Taylor instability and optical properties. *Superlattices Microstruct.* 100:418–30

Ruffino F, Pugliara A, Carria E, Bongiorno C, Spinella C, Grimaldi MG. 2012a. Formation of nanoparticles from laser irradiated Au thin film on SiO_2/Si: elucidating the Rayleigh instability role. *Mater. Lett.* 84:27–30

Ruffino F, Pugliara A, Carria E, Romano L, Bongiorno C, et al. 2012b. Towards a laser fluence dependent nanostructuring of thin Au films on Si by nanosecond laser irradiation. *Appl. Surf. Sci.* 258:9128–37

Sachan R, Malasi A, Ge J, Yadavali S, Krishna H, et al. 2014. Ferroplasmons: intense localized surface plasmons in metal-ferromagnetic nanoparticles. *ACS Nano* 8:9790–98

Sachan R, Yadavali D, Shirato N, Krishna H, Ramos V, et al. 2012. Self-organized bimetallic Ag-Co nanoparticles with tunable localized surface plasmons showing high environmental stability and sensitivity. *Nanotechnology* 23:275604

Schwartz LW. 1998. Hysteretic effects in droplet motion on heterogenous substrates: direct numerical simulation. *Langmuir* 14:3440–53

Seemann R, Herminghaus S, Jacobs K. 2001. Dewetting patterns and molecular forces: a reconciliation. *Phys. Rev. Lett.* 86:5534–37

Seric I, Afkhami S, Kondic L. 2018a. Direct numerical simulation of variable surface tension flows using a volume-of-fluid method. *J. Comput. Phys.* 352:615–36

Seric I, Afkhami S, Kondic L. 2018b. Influence of thermal effects on stability of nanoscale films and filaments on thermally conductive substrates. *Phys. Fluids* 30:012109

Sharma A, Verma R. 2004. Pattern formation and dewetting in thin films of liquids showing complete macroscale wetting: from "pancakes" to "swiss cheese." *Langmuir* 20:10337–45

Sibley D, Nold A, Kalliadasis S. 2013. Unifying binary fluid diffuse-interface models in the sharp interface limit. *J. Fluid Mech.* 736:5–43

Snoeijer JH. 2006. Free-surface flows with large slope: beyond lubrication theory. *Phys. Fluids* 18:021701

Spelt PD. 2005. A level-set approach for simulations of flows with multiple moving contact lines with hysteresis. *J. Comput. Phys.* 207:389–404

Sussman M, Almgren AS, Bell JB, Colella P, Howell LH, Welcome ML. 1999. An adaptive level set approach for incompressible two-phase flows. *J. Comput. Phys.* 148:81–124

Sussman M, Ohta M. 2009. A stable and efficient method for treating surface tension in incompressible two-phase flow. *SIAM J. Sci. Comput.* 31:2447–71

Thiele U, Madruga S, Frastia L. 2007. Decomposition driven interface evolution for layers of binary mixtures. I. Model derivation and stratified base states. *Phys. Fluids* 19:122106

Thompson CV. 2012. Solid-state dewetting of thin films. *Annu. Rev. Mater. Res.* 42:399–434

Trice J, Thomas D, Favazza C, Sureshkumar R, Kalyanaraman R. 2007. Pulsed-laser-induced dewetting in nanoscopic metal films: theory and experiments. *Phys. Rev. B* 75:235439

Trice J, Thomas D, Favazza C, Sureshkumar R, Kalyanaraman R. 2008. Novel self-organization mechanism in ultrathin liquid films: theory and experiment. *Phys. Rev. Lett.* 101:017802

Vogel T, Dodel G, Holzhauer E, Salzmann H, Theurer A. 1992. High-speed switching of far-infrared radiation by photoionization in a semiconductor. *Appl. Opt.* 31:329–37

Wilczek M, Tewes W, Engelnkemper S, Gurevich SV, Thiele U. 2017. Sliding drops: ensemble statistics from single drop bifurcations. *Phys. Rev. Lett.* 119:204501

Williams MB, Davis SH. 1982. Nonlinear theory of film rupture. *J. Colloid Interface Sci.* 90:220–28

Wu Y, Dong N, Fu S, Fowlkes J, Kondic L, et al. 2014. Directed liquid phase assembly of highly ordered metallic nanoparticle arrays. *ACS Appl. Mater. Interfaces* 6:5835–43

Wu Y, Fowlkes JD, Rack PD. 2011a. The optical properties of Cu-Ni nanoparticles produced via pulsed laser dewetting of ultrathin films: the effect of nanoparticle size and composition on the plasmon response. *J. Mater. Res.* 26:277–87

Wu Y, Fowlkes JD, Rack PD, Diez JA, Kondic L. 2010. On the breakup of patterned nanoscale copper rings into droplets via pulsed-laser-induced dewetting: competing liquid-phase instability and transport mechanisms. *Langmuir* 26:11972–79

Wu Y, Fowlkes JD, Roberts NA, Diez JA, Kondic L, et al. 2011b. Competing liquid phase instabilities during pulsed laser induced self-assembly of copper rings into ordered nanoparticle arrays on SiO_2. *Langmuir* 27:13314–23

Wu Y, Li G, Cherqui C, Bigelow NW, Thakkar N, et al. 2016. Electron energy loss spectroscopy study of the full plasmonic spectrum of self-assembled Au-Ag alloy nanoparticles: unraveling size, composition, and substrate effects. *ACS Photonics* 3:130–38

Xia Q, Chou S. 2009. The fabrication of periodic metal nanodot arrays through pulsed laser melting induced fragmentation of metal nanogratings. *Nanotechnology* 20:285310

Yadavali S, Kalyanaraman R. 2014. Nanomaterials synthesis by a novel phenomenon: the nanoscale Rayleigh–Taylor instability. *AIP Adv.* 4:047116

Ye J, Zuev D, Makarov S. 2018. Dewetting mechanisms and their exploitation for the large-scale fabrication of advanced nanophotonic systems. *Int. Mater. Rev.* 64:439–77

Zhao C, Sprittles JE, Lockerby DA. 2019. Revisiting the Rayleigh–Plateau instability for the nanoscale. *J. Fluid Mech.* 861:R3

Annual Review of
Fluid Mechanics

Volume 52, 2020

Contents

Anatol Roshko, 1923–2017
Dimitri Papamoschou and Morteza Gharib 1

David J. Benney: Nonlinear Wave and Instability Processes in Fluid Flows
T.R. Akylas 21

Ocean Wave Interactions with Sea Ice: A Reappraisal
Vernon A. Squire 37

Particles, Drops, and Bubbles Moving Across Sharp Interfaces and Stratified Layers
Jacques Magnaudet and Matthieu J. Mercier 61

Convective Phenomena in Mushy Layers
Daniel M. Anderson and Peter Guba 93

Shear Thickening of Concentrated Suspensions: Recent Developments and Relation to Other Phenomena
Jeffrey F. Morris 121

Subglacial Plumes
Ian J. Hewitt 145

Modeling Turbulent Flows in Porous Media
Brian D. Wood, Xiaoliang He, and Sourabh V. Apte 171

Acoustic Tweezers for Particle and Fluid Micromanipulation
M. Baudoin and J.-L. Thomas 205

Liquid-State Dewetting of Pulsed-Laser-Heated Nanoscale Metal Films and Other Geometries
Lou Kondic, Alejandro G. González, Javier A. Diez, Jason D. Fowlkes, and Philip Rack 235

Capillarity in Soft Porous Solids
Jonghyun Ha and Ho-Young Kim 263

Statics and Dynamics of Soft Wetting
Bruno Andreotti and Jacco H. Snoeijer 285

Turbulence with Large Thermal and Compositional Density Variations
Daniel Livescu 309

Patterns in Wall-Bounded Shear Flows
Laurette S. Tuckerman, Matthew Chantry, and Dwight Barkley 343

Super-Resolution Imaging in Fluid Mechanics Using New Illumination Approaches
Minami Yoda 369

Aeroacoustics of Silent Owl Flight
Justin W. Jaworski and N. Peake 395

Immersed Methods for Fluid–Structure Interaction
Boyce E. Griffith and Neelesh A. Patankar 421

Advances in Bioconvection
Martin A. Bees 449

Machine Learning for Fluid Mechanics
Steven L. Brunton, Bernd R. Noack, and Petros Koumoutsakos 477

Electroconvection near Electrochemical Interfaces: Experiments, Modeling, and Computation
Ali Mani and Karen May Wang 509

Chemo-Hydrodynamic Patterns and Instabilities
A. De Wit 531

Indexes

Cumulative Index of Contributing Authors, Volumes 1–52 557

Cumulative Index of Article Titles, Volumes 1–52 568

Errata

An online log of corrections to *Annual Review of Fluid Mechanics* articles may be found at http://www.annualreviews.org/errata/fluid